Mitochondrial and cellular function in fibroblasts, induced neurons, and astrocytes derived from case study patients: insights into major depression as a mitochondria-associated disease

Christian Wetzel (christian.wetzel@ukr.de)
University of Regensburg https://orcid.org/0000-0002-5762-0003
Iseline Cardon
University of Regensburg https://orcid.org/0000-0001-5533-4727
Sonja Grobecker
University of Regensburg
Selin Kücükoktay
University of Regensburg
Stefanie Bader
Tatjana Jahner
Caroline Nothdurfter
University of Regensburg
Kevin-Thomas Koschitzki
Mark Berneburg
Regensburg University Hospital
Heidi Stöhr
Bernhard Weber
Marcus Höring
Gerhard Liebisch
Frank Braun
Tanja Rothammer-Hampl
Markus Riemenschneider
Regensburg University Hospital
Rainer Rupprecht
Vladimir Milenkovic

Article

Keywords: major depressive disorder, mitochondrial functions, mitochondriopathy, treatment-resistant depression, iPS-neurons, iPS-astrocytes

Posted Date: November 22nd, 2023

DOI: https://doi.org/10.21203/rs.3.rs-3125187/v2

Additional Declarations:
The authors have declared there is **NO** conflict of interest to disclose

Article

Mitochondrial and cellular function in fibroblasts, induced neurons, and astrocytes derived from case study patients: insights into major depression as a mitochondria-associated disease

Iseline Cardon[1], Sonja Grobecker[1], Selin Kücükoktay[1], Stefanie Bader[1], Tatjana Jahner[1], Caroline Nothdurfter[1], Kevin Koschitzki[2], Mark Berneburg[2], Bernhard H.F. Weber[3,4], Heidi Stöhr[3], Marcus Höring[5], Gerhard Liebisch[5], Frank Braun[6], Tanja Rothhammer-Hampl[6], Markus J. Riemenschneider[6], Rainer Rupprecht[1], Vladimir M. Milenkovic[1], Christian H. Wetzel[1*]

[1] Department of Psychiatry and Psychotherapy, University of Regensburg, 93053 Regensburg, Germany
[2] Department of Dermatology, Regensburg University Hospital, 93053 Regensburg, Germany
[3] Institute of Human Genetics, University of Regensburg, 93053 Regensburg, Germany
[4] Institute of Clinical Human Genetics, Regensburg University Hospital, 93053 Regensburg, Germany
[5] Institute of Clinical Chemistry and Laboratory Medicine, Regensburg University Hospital, 93053 Regensburg, Germany
[6] Department of Neuropathology, Regensburg University Hospital, 93053 Regensburg, Germany
*Correspondence: Christian.Wetzel@ukr.de; Tel.: +49 941 944 8955

Abstract: Background: The link between mitochondria and major depressive disorder (MDD) is increasingly evident, underscored both by mitochondria's involvement in many mechanisms identified in depression, and high prevalence of MDD in individuals with mitochondrial disorders. Mitochondrial functions and energy metabolism are increasingly considered to be involved in MDD's pathogenesis. This study focused on cellular and mitochondrial (dys)function in two atypical cases: an antidepressant non-responding MDD patient ("Non-R") and another with an unexplained mitochondrial disorder ("Mito"). Methods: Skin biopsies from these patients and controls were used to generate various cell types, including astrocytes and neurons, and cellular and mitochondrial functions were analyzed. Results: Similarities were observed between the Mito patient and a broader MDD cohort, including decreased respiration and mitochondrial function. Conversely, the Non-R patient exhibited increased respiratory rates, mitochondrial calcium, and resting membrane potential. Conclusions: The Non-R patient's data offered a new perspective on MDD, suggesting a detrimental imbalance in mitochondrial and cellular processes, rather than simply reduced functions. Meanwhile, the Mito patient's data revealed the extensive effects of mitochondrial dysfunctions on cellular functions, potentially highlighting new MDD-associated impairments. Together, these case studies enhance our comprehension of MDD.

Keywords: major depressive disorder; mitochondrial functions; mitochondriopathy; treatment-resistant depression; iPS-neurons; iPS-astrocytes

1. Introduction

Depression is a major public health challenge and a leading cause of disability [1]. In a recent study, Liu *et al.* showed that the number of incident cases of depression worldwide rose by almost 50% from 1990 to 2017 [2]. As of 2019, 280 million people were living with depressive disorders worldwide [3]. Among them, 193 million people suffered from

major depressive disorder (MDD), and this number has surged by 26% as a result of the COVID-19 pandemic, reaching a staggering 246 million people. Therefore, studying MDD appears increasingly relevant.

Although the precise pathomechanisms underlying MDD development are still not completely understood, various hypotheses have been put forward. One of the oldest and widely accepted hypotheses describes the dysregulation of neurotransmission, especially in the monoaminergic system. Reduced neuroplasticity resulting from impaired BDNF signaling has also been reported [4]. In line with the first hypothesis, common antidepressant (AD) treatments aim to compensate the reduced monoamine neurotransmitters in the synaptic cleft. However, in a recent study, Casarotto *et al*. demonstrated that their clinical effect is most likely mediated by their binding to the neurotrophin receptor TRKB [5].

Yet, for primary AD treatments the remission rate ranges between 30 and 45% [6]. The mechanisms of AD resistance are not completely clear, but a number of predictors for AD response have been identified [7]. Among them, drug metabolism, mediated primarily by cytochrome P450 enzymes in the liver, plays a critical role. Other predictors include environmental factors, drug efflux transporters present on the blood brain barrier, neurotransmission and HPA axis activity [7].

Beyond the monoamine hypothesis, mitochondria and energy metabolism have turned into focus in the pathomechanisms of depression [8-11]. Mitochondrial dysfunction, resulting in decreased energetic capacity, oxidative stress, and alterations in signaling, is regarded as a key risk factor for MDD and other psychiatric disorders [9-12].

Neurons display a very high energy demand as a consequence of respective physiological processes. Remarkably, it is estimated that 75% of the total adenosine triphosphate (ATP) consumption in the brain serves to maintain resting membrane potential, which is critical for membrane excitability and neurotransmission [13]. Consequently, neurons are highly vulnerable to metabolic stress.

Typical examples of metabolic stress are mitochondrial diseases (MDs). MDs result from dysfunctional mitochondria and form a group of clinically heterogeneous genetic disorders [14]. MDs are far more frequent than previously assumed. Schaefer *et al*. estimated a prevalence of 9,2 mitochondrial DNA diseases per 100,000 adults [15]. In children below 16 years of age, the estimated prevalence of MDs ranges from 5 to 15 cases per 100,000 individuals [14]. However, mitochondrial disorders are hard to define in children and induce unspecific symptoms, making misdiagnoses likely and possibly resulting in underdiagnosed MDs [16]. Predominantly, MDs lead to defects in oxidative phosphorylation. Such shortcomings can affect any tissue, although those requiring high levels of energy, such as muscle and brain, are most severely affected. Symptoms can encompass non-neurological or neurological manifestations and typically involve multiple organ systems [14].

However, the most commonly affected structure in MDs is the nervous system, with symptoms including stroke-like episodes, migraine, epilepsy, spasticity and ataxia, visual impairment, hearing loss, intellectual disability, and fluctuating encephalopathy [17]. Brain dysfunction in MDs can also lead to neuropsychological or psychiatric disturbances. Indeed, Morava *et al*. showed that 70% of MD patients will experience a major mental illness at some point during their live [18]. Moreover, Fattal *et al*. reported depressive behavior in 50% of children with a MD [19].

Interestingly, in a case series in MD, Anglin *et al*. reported that 11 out of 12 patients presented treatment-resistant psychiatric illnesses [20]. Furthermore, clinical deterioration upon psychotropic medication treatment has been shown in patients with MDs [20, 21]. Many psychotropic drugs are known to impair mitochondrial functions [22], although, as Riquin *et al*. pointed out, “it is challenging to delineate whether mitochondrial dysfunction occurs secondary to pharmaceutical treatment or whether it is a result of the underlying disease process itself” [21]. These observations highlight the need to consider MDs in patients diagnosed with psychiatric illnesses, such as MDD, and to adapt treatment accordingly.

On the one hand, neurons are highly vulnerable to metabolic stress, including MDs, which can lead to psychiatric illness such as MDD. On the other hand, mitochondrial impairments associated with MDD have been reported in peripheral cells such as muscle cells [23] , platelets [24, 25], peripheral blood mononuclear cells [26] and fibroblasts [27, 28]. As a result, it is becoming increasingly clear that MDD is not merely limited to mental afflictions but also encompasses physical manifestations. This emphasizes the importance to consider MDD-associated pathomechanisms in neuronal as well as non-neuronal cells. Therefore, we studied a human cellular model of MDD in order to unravel the molecular pathomechanisms related to mitochondrial dysfunction and bioenergetics imbalance. In a previous study, we collected dermal fibroblasts from MDD patients and non-depressed controls and demonstrated a clear mitochondrial impairment, including reduced respiration and ATP content [28]. We then reprogrammed the fibroblasts to induced pluripotent stem cells (iPSCs), which we subsequently differentiated to neural progenitor cells (NPCs) and neurons [29]. Like in peripheral cells, we observed signs of altered mitochondrial function in the neural lineage including lower respiration rates. In neurons, electrophysiological measurements showed significantly lower membrane capacitance, a more depolarized membrane potential, and increased spontaneous electrical activity [29]. Moreover, astrocyte pathology has been reported in human post-mortem brain tissue of MDD patients [30], suggesting that these glial cells also play a role in the etiology of depression. Therefore, in the present study, we extended our human depression model to iPSC-derived astrocytes.

The aim of the present study was to build on the above-mentioned cohort studies and complement them with case studies, in order to extend our knowledge on the biological mechanisms underpinning the development of MDD [28, 29]. Case studies are detailed, intensive studies that seek to explain particular cases and understand causal mechanisms and processes. They allow an in-depth understanding of the factors under study. The focus on outlier cases who do not fit the general theory brings the potential to help understand mechanisms that had not been explored before. Where cohort studies measure a lot of cases with a limited number of parameters, case studies aim at measuring a few cases very precisely to understand the interplay between different parameters. Here, we investigated an anti-depressant (AD) non-responder MDD patient and a non-depressed mitochondriopathy patient, in order to gain new perspectives on MDD in the context of the bioenergetics hypothesis of psychiatric disorders.

The first patient was defined as AD non-responder after three treatment regimens failed to induce remission over twelve weeks, according to the most accepted definition of treatment resistant depression (TRD) (see Table 1 for patient information) [7, 31]. In contrast with patients from the MDD cohort who all achieved a certain degree of remission (average remission 58±7%), the Non-R patient still suffered from severe MDD at the time of the biopsy. Studying this patient was therefore an opportunity to investigate how cellular and mitochondrial functions differed between remitted, treatment-responding MDD patients and a severely depressed, treatment-resistant MDD patient.

The mitochondriopathy patient presented several neurological symptoms, somatic symptoms, and physical pains. She was directed to the Center for Rare Diseases, Regensburg, Germany, where a series of tests allowed to rule out several pathologies and disorders (see Table 1 for patient information). As certain symptoms pointed towards a mitochondrial disorder, exome and mitochondrial genome were sequenced, and showed no mitochondrial disease-associated mutations. However, blood tests revealed strong alterations in several factors that play a critical role in mitochondrial function. Studying this patient was an opportunity to observe the interplay between different cellular and mitochondrial parameters and compare them in the context of a mitochondriopathy and of MDD. A further aim was to understand how specific cellular processes and characteristics that could be altered in depression were influenced by mitochondrial (dys)function. This case study was therefore relevant to our understanding of different aspects of MDD pathophysiology related to mitochondria.

We investigated cellular and mitochondrial functions in fibroblasts, NPCs, astrocytes, and neurons derived from these two patients and their matched healthy controls. In those different cell types, bioenergetic functions were assessed by measuring mitochondrial respiration, ATP content, substrate availability, mitochondrial content, cell size and MMP. Mitochondrial and cytosolic Ca^{2+} levels were measured. Oxidative stress was investigated by measuring mitochondrial and cellular reactive oxygen species (ROS), lipid peroxidation and antioxidant capacity of the glutathione system. Moreover, we analyzed electrophysiological properties of neurons using whole-cell voltage- and current-clamp measurements.

Table 1. Patients information

<table>
<tr><td></td><td colspan="3">Non-responder patient</td></tr>
<tr><td>Age, sex</td><td colspan="3">43, male</td></tr>
<tr><td rowspan="2">Clinical findings</td><td colspan="2">Symptoms</td><td>Ratings</td></tr>
<tr><td colspan="2">- Depressive mood
- Guilt feelings
- Suicide ideation
- Insomnia and disturbed sleep
- Severe somatic symptoms of anxiety
- Loss of appetite and weight loss
- Loss of interest in any activity</td><td>- Hamilton Depression Rating score at the beginning of the in-patient stay at the clinic: 34 (very severe)
- Hamilton Depression Rating score after 2 months and several treatments attempts : 22 (severe)</td></tr>
<tr><td>Treatments</td><td colspan="3">Antidepressants
- Duloxetine
- Venlafaxine
- Venlafaxine + lithium
Others
- Enalapril (hypertension)</td></tr>
<tr><td></td><td colspan="3">Mitochondriopathy patient</td></tr>
<tr><td>Age, sex</td><td colspan="3">18, female</td></tr>
<tr><td rowspan="2">Clinical findings</td><td colspan="2">Symptoms</td><td>Excluded pathologies</td></tr>
<tr><td colspan="2">- Fatigue and hypersomnia
- Migraines
- Pain in wrist, back, shoulders, feet, fingers, elbows, hips
- Numbness in arms and legs
- Paresthesia in arms and legs
- Loss of visual acuity: myopie and hypermetropie
- Gastointestinal symptoms : nausea, vomitting, diarrhea</td><td>- Inflammatory bowel disease
- Immune-related diseases
- Thyroid disorders
- Ankylosing spondylitis
- Rheumatoid arthritis
- Osteoporosis
- Borreliosis
- Optic neuritis
- Sacroiliitis
- Orthopedic problems
- Sarcoma
- Neuroblastoma</td></tr>
<tr><td rowspan="5">Blood tests relevant to diagnosis</td><td>Measured parameter</td><td>Alteration</td><td>Description</td></tr>
<tr><td>LDH2</td><td>Decreased</td><td rowspan="2">Enzymes involved in lactate metabolism</td></tr>
<tr><td>LDH4</td><td>Increased</td></tr>
<tr><td>Citrate</td><td>Starkly decreased</td><td rowspan="2">Enzymes involved in tricarboxylic acid cycle</td></tr>
<tr><td>Cis-aconitate</td><td>Starkly decreased</td></tr>
</table>

	Isocitrate	Starkly decreased	
	Pyruvate kinase M2	Increased	Enzyme catalysing the last step of glycolysis
	Vitamine D3	Decreased	Regulator of mitochondrial respiration and oxidative stress
	Coenzyme Q10	Decreased	Electron carrier in the electron transport chain
Urine test	5-Hydroxyindolacetatic acid	Starkly decreased	Serotonin metabolite, low levels linked with depression

2. Materials and Methods

2.1 Generation of control and MDD patient iPSCs from fibroblasts

Skin biopsies were conducted by the Department of Dermatology, Regensburg University Hospital, Germany. The study was approved by University of Regensburg's ethics committee (ref: 13-101-0271), all participants provided written informed consent. Human fibroblasts were obtained and cultivated as previously described [28]. Fibroblasts from healthy age- and sex-matched controls were also obtained. The non-responder patient is hereafter referred to as "Non-R" and the corresponding control as "Ctl 17". The mitochondriopathy patient is referred to as "Mito" and the corresponding control as "Ctl 18".

iPSCs were generated using the episomal protocol described by [32]. Briefly, $5x10^5$ fibroblasts were electroporated with 600 ng of each the episomal vectors pCBX-EBNS, pCE-hsk, pCE-hUL, pCE-hOCT3/4 and pCE-mp53DD using the Amaxa Nucleofactor (Lonza). The cells were then cultured in TeSR-E7 medium on Matrigel-coated dishes (Corning) until colonies appeared. iPSC colonies were manually picked and cultured on Matrigel with mTeSR1 medium.

2.2 iPSC differentiation to NPCs and neuron differentiation

iPSCs to neural progenitor cells (NPCs) differentiation was carried out following a monolayer culture method developed by Yan *et al.* [32]. Small iPSCs colonies were plated on Matrigel-coated plates in Neural Induction Medium (Neurobasal Medium, 2% Neural Induction Supplement, 0,5% Penicillin/Streptomycin). On day 7, the differentiating cells were dissociated using Accutase (Life Technologies), passed through a 50 μm strainer and further cultured in Neural Expansion Medium (Neurobasal/Advanced DMED F12, 2% Neural Induction Supplement, 0,5% Penicillin/Streptomycin) on Geltrex-coated plates. After 5 passages, a pure culture of mature NPCs was obtained.

For neuronal differentiation, $3.5x10^4$ NPCs from passage 5 to 12 onto polymer imaging μ-dishes (Ibidi) coated with 20% poly-L-ornithine in PBS and 43 μg/mL laminin in DMEM/F12, both overnight at 37°C. On the next day, medium was changed to Neurobasal medium with 1% B27, 0.5% GlutaMax, 0.5% non-essential amino acids, 0.5% Culture One (Thermo Fisher Scientific), 200 nM ascorbic acid (Carl Roth), 20 ng/ml BDNF and GDNF (PeproTech), 1 mM dibutyryl-cAMP (Stemcell), 4 μg/ml laminin (Sigma) and 50 U/ml penicillin, 50 μg/ml streptomycin (Thermo Fisher Scientific). Cells were differentiated for 21 days, with half of the medium changed every 3 to 4 days. In order to remove proliferating cells, the cultures were treated with the mitotic inhibitor cytarabine (Biomol) at 1μM from day 5 to day 6 or 7.

2.3 Astrocytes differentiation

NPCs were differentiated into astrocytes following a protocol adapted from [33]. $3x10^4$ carefully dissociated NPCs were seeded on Matrigel coated plates in astrocytes media containing 2% FBS, 1% astrocytes growth supplement and 1% penicillin/streptomycin solution (ScienCell). Upon confluence, cells were detached and $3x10^4$ cells were plated in new wells. After 30 days of differentiation, identity and maturity of the astrocytes were

confirmed with immunostainings of typical astrocytes markers (GFAP, S100β, connexin 43, EAAT1, ALDH1L1). Astrocytes were grown on Matrigel-coated plates and used until day 60.

2.4 Analysis of mitochondrial respiration

Mitochondrial respiration was analyzed using Seahorse XFp Flux analyzer with a Seahorse XFp Mito Stress Test Kit (Agilent Technologies) according to manufacturer´s recommendations. The day prior the assay, $3x10^4$ (fibroblasts, astrocytes) or $8x10^4$ (NPCs) cells were grown in XFp 8-well miniplates with appropriate coating. Oxygen consumption rates (OCR) were measured with sequential injection of 1 μM oligomycin, 2 μM (fibroblasts, astrocytes) or 1 μM FCCP (NPCs), and each 0.5 μM rotenone/antimycin A (Biomol). Respiration rates were normalized to the number of cells.

2.5 Immunofluorescence

Immunofluorescence stainings were carried out as described in [29]. Primary antibodies used were: anti-β-III-tubulin (mouse; 1:2000, G7121, Promega,), anti-MAP2 (chicken; 1:5000, ab5392, Abcam), anti-VGLUT1 (rabbit; 1:500, ab180188, Abcam), anti-Neun (rabbit; 1:500, ab177487, Abcam), anti-ALDH1L1 (rabbit, 1:500, ab87117, Abcam), anti-EAAT1 (rabbit, 1:200, ab416-1001, Abcam), anti-GFAP (mouse, 1:400, C53893, Sigma-Aldrich), and anti-Connexin 43 (mouse, 1:500, 14-4759-82, Invitrogen). Secondary antibodies used were: anti-mouse Cy3 (1:1000; Thermo Fisher Scientific), anti-rabbit 488, anti-chicken Cy5 (1:1000, Abcam). Nuclei were stained with DAPI (1:1000; Sigma-Aldrich) and coverslips were mounted using Dako Fluorescing Mounting Medium.

2.6 Luminescent assay for ATP content

For the quantification of cellular ATP content, $1x10^5$ fibroblasts and astrocytes or $1x10^6$ NPCs were pelleted and stored at -20 °C. ATP content was measured by CellTiter-Glo®Cell Viability Kit (Promega) according to manufacturer's instructions. Cell pellets were resuspended in 500 μl PBS, heated at 100 °C for 2 min and kept on ice. Triplicates of 50 μl of sample or standard were applied to a 96-well-plate with 50 μl of CellTiter-Glo®Reagent. Luminescence was measured at an integration time of 1 sec. The RLU was used to calculate the ATP content using a 1 nM to 10 μM standard curve. Concentrations were normalized to μg/mL protein using a BCA assay (Thermo Fisher Scientific).

2.7 Luminescent assay for NAD/NADH ratio

To measure substrate availability, $5x10^2$ fibroblasts or $5x10^3$ NPCs were seeded in duplicates 96-wells plates. NAD/NADH ratio was measured with NAD/NADH-Glo™ assay (Promega) according to manufacturer's instructions. Briefly, cells are lysed in a base solution containing dodecyltrimethylammonium bromide. For NAD^+ detection, 0.4N HCl was added to the lysis solution, and the plate was heated at 60 °C for 15 min. Then, NAD^+ and NADH wells were buffered with Trizma® and HCl/Trizma® solution respectively. NAD/NADH-Glo™ detection reagent was added and incubated for 30 min before recording luminescence.

2.8 Luminescent assay for GSH/GSSG ratio

Reduced and oxidized forms of glutathione were measured with the GSH/GSSG-Glo™ assay (Promega) according to manufacturer's instructions. $5x10^2$ fibroblasts were seeded in duplicates in 96-wells plates. The next day, cells were lysed with either total or oxidized glutathione lysis reagent for 5 min on a plate shaker at room temperature (RT). Luciferin generation and detection reagents were subsequently added and incubated at RT for 30 and 15 min, respectively, before recording luminescence.

2.9 Lipid peroxidation ELISA

The levels of the lipid peroxidation marker 8-isoprostane were measured in fibroblasts and NPCs culture supernatants, using the 8-isoprostane ELISA Kit (Cayman Chemicals) according to manufacturer's instructions. Fibroblasts or NPCs were plated in serum-free medium. Upon confluence, cells were detached and counted, while supernatants

were collected. Supernatants were frozen with 1:1000 antioxidant butylated hydroxytoluene to avoid lipids degradation. Supernatants were measured in triplicates in the ELISA plate. 8-isoprostane concentrations were calculated using a standard curve and normalized to the number of cells.

2.10 Imaging of mitochondrial membrane potential (JC-1) cytosolic Ca^{2+} (Fura-2/AM) and mitochondrial Ca^{2+} (Rhod-2/AM)

Live-cell imaging experiments were performed using Zeiss Axio Observer Z.1 microscope equipped with a Fluar 40/1.3 objective lens (Zeiss). All recordings were performed with an AxioCam MRm CCD camera (Zeiss) and a 40X oil immersion objective. The Lambda DG-4 high-speed wavelength switcher (Sutter Instruments) was used for illumination and image acquisition and the microscope was controlled using the ZEN 2012 imaging software. For the analysis, regions of interest were manually drawn around cells using ImageJ (version 2.9.2) [34, 35]. Macros were used for background subtraction, and, where applicable, to calculate ratios, in order to ensure the repeatability of the analysis. Additionally, cell size was measured in Fura-2/AM-loaded cells.

The day before experiments, $1.5x10^5$ fibroblasts, $1.5x10^5$ astrocytes or $2x10^6$ NPCs were plated on uncoated, Matrigel- or Geltrex-coated glass coverslips, respectively. For neurons, $3.5x10^4$ NPCs were plated, and differentiated for 21 days on PLO/laminin-coated Ibidi dishes. For MMP measurement, cells were loaded with JC-1 at a concentration of 300 nM in fibroblasts and astrocytes, and 1 μM in NPCs and neurons. For calcium measurements, cells were loaded with 2 μM Fura-2/AM and 2 μM Rhod-2/AM in OptiMem. Cells were incubated at 37 °C for 30 min. JC-1 fluorescence was measured at 537/42 nm (green) and 620/60 nm (red), after excitation at 480/36 nm. In neurons, neurites and somas appeared on different focus planes, and were imaged separately.

Fura-2 fluorescence was measured at 510 nm after excitation at 340 or 380 nm. Rhod-2 fluorescence was measured at 576 nm after excitation at 556 nm. In neurons, in addition to basal cytosolic Ca2+ measurements, spontaneous Ca^{2+} peaks were recorded over 20 min with 2 Hz frequency using the Fluar 20X/0.75 objective lens. Spikes were analyzed with the software IGOR Pro 9 (WaveMetrics).

2.11 Flow cytometry (MitoTracker Green, DCFDA, MitoSOX)

Flow cytometry was used to detect ROS and mitochondrial content in fibroblasts, NPCs and astrocytes using specific fluorescent dye. DCFDA (2',7'-dichlorofluorescein diacetate) (10μM, 20 min) was used to detect cytosolic hydrogen peroxide and peroxyl radicals, mitochondrial superoxide was detected with MitoSOX (5 μM, 30 min), and mitochondrial mass was investigated using MitoTracker Green (1 μM, 1h). For MitoTracker Green staining, cyclosporine A 500 μg/mL was used to prevent mitochondria depolarization. $2x10^4$ events were recorded for fibroblasts and astrocytes, and $1x10^5$ events were recorded for NPCs. Samples were acquired with the FACS Celesta™ Cell Analyzer and analyzed using FlowJo software (V10.8, Tree Star).

2.12 Electrophysiology

Whole-cell patch-clamp recordings were performed on induced neurons during their 4th week of differentiation. The extracellular solution was composed of 140 mM NaCl, 5 mM KCl, 2 mM $CaCl_2$, 1 mM $MgCl_2$, 10 mM HEPES, and 5 mM Glucose, pH 7.3. Micropipettes were made of borosilicate glass (Science Products) by means of a horizontal pipette puller (Zeitz Instruments) and fire-polished to obtain a series resistance of 3-5 MΩ. Micropipettes were filled with intracellular solution (140 mM KCl, 1 mM $MgCl_2$, 0.1 mM $CaCl_2$, 5 mM EGTA, 10 mM HEPES). Recordings were made using a HEKA Electronic EPC-10 amplifier (HEKA Electronic). The liquid-liquid junction potential was calculated to be 4 mV (LJP calculator of the pClamp software suite, Axon Instruments) but not corrected. The series resistance was assessed but not compensated. The resting membrane potential (RMP) and capacitance were recorded directly after reaching the whole-cell configuration. For voltage-clamp recordings, membrane potential was held at -80 mV and

depolarized in steps of 10 mV to evoke voltage-activated Na^+- and K^+-channels. Spontaneous post-synaptic currents were recorded while holding the membrane potential at –80 mV. In current-clamp mode, manually adjusted currents were injected to hyperpolarize the membrane potential to about -80 mV or –50 mV and to record spontaneous action potentials. All patch-clamp recordings were carried out at room temperature. Data were analyzed using Patchmaster Next (HEKA Electronic). Cells with RMP of 0 mV and above were excluded from the analysis.

2.13 Statistical analysis

Graphical depiction and statistical analysis were conducted with Graph Pad Prism 9.5.1 (GraphPad Software). For all experiments, except patch-clamp recordings, the means of two to three technical replicates were calculated and two to three biological replicates were averaged. A technical replicate refers to the same experimental procedure being repeated multiple times on the same sample. Biological replicates refer to independent samples. Measurements were conducted pairwise allowing direct comparison. Statistical outliers were detected and eliminated using ROUT-Method, except for the number of events in spontaneous activity experiments (post-synaptic currents and action potentials). Results of spontaneous activity were compared by Fisher's exact test. All results showed variance homogeneity and were compared using paired Student's *t*-Test. Results were presented as mean ± SEM. *p*-value limit for statistical significance was set to ≤ 0.05. Table S1, S3, S4, S6 and S7 present mean ± SEM, n and *p*-value for each comparison.

3. Results

To investigate the neurobiological underpinnings of major depressive disorder (MDD) we are studying cellular and mitochondrial function in human cellular models. We characterized dermal fibroblasts [28] and generated induced pluripotent stem cells (iPSCs), which were further differentiated to neural progenitors (NPCs) and induced neurons [29].

To extend our knowledge on the involvement of mitochondrial dysfunction in MDD in the present work we studied two specific patients, one suffering from a suspected mitochondriopathy ("Mito"), and one antidepressant non-responding MDD patient ("Non-R"). The results from these case study patients are directly compared to respective controls and to changes observed between MDD and control cohorts [28, 29].

Further information on MDD study participants can be found in the METHODS and in [28, 29]. Exome sequencing of the Mito and Non-R patient fibroblast gDNA did not reveal any known disease-associated variants (point mutations or indels) (data not shown but will be provided on request).

3.1. Fibroblasts from the antidepressant non-responder (Non-R) and the mitochondriopathy patient (Mito) show altered bioenergetic properties

To investigate the activity of the oxidative phosphorylation system (OXPHOS) as a key function of mitochondrial metabolism, we measured the oxygen consumption rate (OCR) in the fibroblasts of patients and of the sex- and age-matched controls. In the Mito patient, OCR was significantly decreased across most assessed parameters. Likewise, patients from the MDD cohort exhibited a lower OCR in most parameters (Figure 1A, Table S1). Surprisingly, the antidepressant non-responder patient (Non-R) showed markedly increased maximal respiration, spare respiratory capacity and proton leak when compared to its matched control and to the MDD and control cohort (Figure 1A, Table S1).

Although OXPHOS activity significantly varies in patient fibroblasts, we did not detect differences in the cellular content of ATP, the NAD/NADH ratio, and the mitochondrial content (Figure 1B, Table S1).

The mitochondrial membrane potential (MMP) is indicative of the proton motive force and indirectly reflects the metabolic activity and capacity of mitochondria. It can be assessed by labelling mitochondria with the potential-dependent ratiometric dye JC-1. Like the MDD patients, the Mito patient showed a lower MMP than the non-depressed control (Figure 1C, Table S1). However, despite highly increased respiration, the MMP was not significantly different in the Non-R patient (Figure 1C, Table S1).

The cellular Ca^{2+} homeostasis is affected by energy-demanding active transport processes and dependent on chemical and electrical gradients. Ca^{2+} levels also have regulatory effects on signaling, enzyme function and metabolism. Using the Ca^{2+} sensitive dyes Fura-2/AM and Rhod-2/AM, we investigated cytosolic and mitochondrial Ca^{2+} levels, respectively. Consistent with results from the MDD cohort fibroblasts, no significant differences were observed in the cytosolic Ca^{2+} levels in our case study patients (Figure 1C, Table S1). However, alongside increased respiration, a marked increase in mitochondrial Ca^{2+} was found in the Non-R patient, while there was no change in the Mito patient (Figure 1C, Table S1).

Like in the MDD cohort, the patients' fibroblasts were significantly smaller than the control cells when assessed in Fura-2/AM loaded cells (Figure 1D, Table S1). This finding is consistent with the hypothesis of a metabolic/bioenergetic dysregulation in patient cells which could also lead to morphological changes.

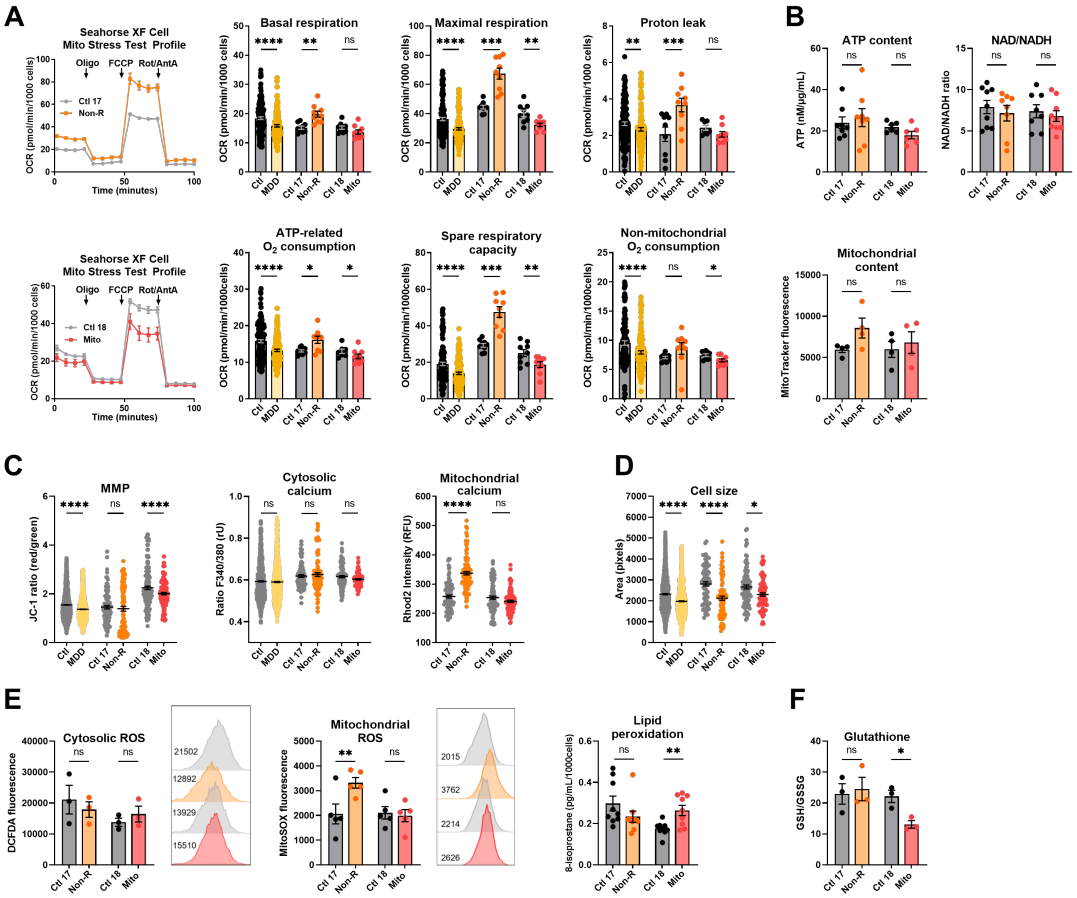

Figure 1. Mitochondrial bioenergetics in fibroblasts. (A) Mitochondrial respiration. The oxygen consumption rate (OCR) was measured following the Agilent XF Mito Stress Test protocol consisting of sequential injections of oligomycin (Oligo), carbonyl cyanide-4-(trifluoromethoxy)-phenylhydrazone (FCCP) and rotenone/antimycin A (Rot/AntA) to reveal different respiratory parameters. Left: representative OCR curves for Ctl 17/Non-R (above) and Ctl 18/Mito (below). Right: OCR of control and patient's fibroblasts in key respiratory parameters. Bar plots show normalized mean

OCR values ± SEM. **(B) Bioenergetics parameters.** *ATP content* was measured using a luminescent assay and normalized to protein amount. Bar plot shows nM ATP per μg/mL proteins ± SEM. Substrate availability was estimated by measuring the *NAD/NADH ratio* with a colorimetric assay. Bar plots represent mean NAD/NADH ratio ± SEM. *Mitochondrial content* was measured by flow cytometry and is indicated by MitoTracker Green mean fluorescence ± SEM, $2x10^4$ events were recorded for each replicate. **(C) MMP and calcium homeostasis.** *MMP* was measured with the JC-1 dye and is indicated by the fluorescence ratio between JC-1 aggregates (red) over JC-1 monomers (green). Dot plot shows mean red/green ratios ± SEM. *Cytosolic calcium* was measured as the Fura-2 fluorescence ratio F340/380 and is represented as mean ratio ± SEM. *Mitochondrial calcium* levels were measured using Rhod-2/AM and is presented as mean fluorescence intensity, in relative fluorescent unit ± SEM. **(D) Cell size** was analyzed by assessing area (pixels) of Fura-2/AM-loaded cells. Dot plot shows the number of pixels ± SEM. **(E) Oxidative stress indicators.** Cytosolic reactive oxygen species (ROS) and mitochondrial ROS (superoxide) were measured by flow cytometry and are indicated by DCFDA and MitoSOX mean fluorescence, respectively. Bar plots show mean fluorescence ± SEM, $2x10^4$ events were recorded for each replicate. On the right of each graph, with matching colour coding and order, are representative histograms showing fluorescence (x-axis) and cell count (y-axis). Numbers indicate mean fluorescence. Lipid peroxidation was estimated by measuring 8-isoprostane concentration in cell culture supernatant and normalized to the number of cells. Bar plot shows mean 8-isoprostane concentration in pg/mL/1000 cells ± SEM. **(F) Antioxidant system** function was estimated with the ratio of reduced (GSH) to oxidized (GSSG) glutathione using a luminescent assay. Bar plots show the mean ratio GSH/GSSG ± SEM. Ctl: non-depressed controls cohort; MDD: major depressive disorder cohort; Ctl 17 and Ctl 18: non-depressed controls; Non-R: non-responder patient; Mito: mitochondriopathy patient. All data were analyzed with paired t-test, significant differences were indicated with * ($p<0.05$), ** ($p<0.005$), *** ($p<0.0005$) and **** ($p<0.0001$). Mean, SEM, n and *p*-value are compiled in Table S1.

3.2. Redox homeostasis is partly affected in AD Non-R and Mito patient fibroblasts

Reactive oxygen species (ROS) exert important signaling functions, but also cause oxidative stress leading to molecular damage. Mitochondria are major players in the maintenance of the cell's redox homeostasis by generating ROS at complex I and III of the ETC. ROS also occur in the cytosol, where they can cause lipid peroxidation. The redox balance is maintained by the antioxidant system, including glutathione.

We measured cytosolic ROS and mitochondrial superoxide by flow cytometry using the DCFDA and MitoSOX dyes, respectively. No significant difference appeared in the cytosolic ROS content of fibroblasts, but mitochondrial superoxide levels were significantly increased in fibroblasts from the Non-R patient (Figure 1E, Table S1). Such increase is consistent with a hyperactive ETC, as observed in the respirometry experiments (Figure 1A, Table S1).

Lipid peroxidation was estimated by measuring one of its main by-products, 8-isoprostane, and was shown to be significantly increased in fibroblasts from the Mito patient. Assessing the glutathione oxidation with a luminescence-based kit revealed a significantly lower GSH/GSSG ratio in the Mito patient's fibroblasts. This suggests a potential oxidative stress and lower antioxidant capacity in the Mito patient's cells (Figure 1F, Table S1).

A broader analysis of cellular and mitochondrial lipids using an untargeted lipidomics approach did not reveal any marked alterations in the lipid composition of Mito or Non-R patient cells (data not shown; identification and quantification of detected lipid species will be provided on request).

3.3. Induced neural progenitor cells of patients show alterations in bioenergetic properties

To further investigate bioenergetic properties of neural cells we used the patients' primary skin fibroblasts and reprogrammed them to iPSCs by transient episomal transduction according to the Yamanaka protocol [36, 37]. iPSCs were differentiated to NPCs and stained for the neural progenitor markers SOX2 and PAX6 [38] (Figure 2A). Table S2 shows that most cells co-express both markers.

NPCs from the MDD cohort had significantly lower respiration in all parameters measured (Figure 2B, Table S3). Like in fibroblasts, NPCs from the Non-R patient showed

significantly increased OCR in basal and maximal respiration, increased proton leak and ATP-related oxygen consumption. NPCs from the Mito patient had lower OCR, with a significant decrease in maximal respiration and spare respiratory capacity (Figure 2B, Table S3).

Cellular ATP levels and mitochondrial content were not significantly different in the NPCs of patients and their respective controls (Figure 2C, Table S3). However, a NAD/NADH ratio elevation was identified in both patients, yet statistical significance was reached only in the Mito patient (Figure 2C, Table S3), indicating that substrate availability might be affected in patients' NPCs.

In NPCs of the Non-R patient and the MDD cohort, the MMP did not significantly differ from the controls). However, a significant increase was observed between the Mito patient and its control. Cytoplasmic Ca^{2+} levels in NPCs were higher in both the Mito patient and the MDD cohort, while they did not differ between the Non-R patient and Ctl 17. In contrast, mitochondrial Ca^{2+} levels were higher in the Non-R patient NPCs and lower in the Mito patient. (Figure 2D, Table S3).

Consistent with observations in fibroblasts, NPCs were significantly smaller in the Mito and Non-R patients, and in the MDD cohort, when compared to their controls (Figure 2E, Table S3).

While there was no clear difference in cellular ROS between NPCs of patients and controls, as observed in fibroblasts, NPCs from the Mito patient showed a significant increase in mitochondrial superoxide (Figure 2F, Table S3). Despite a high interindividual variability between the controls, potentially attributable to the age difference (see Table 1 for patients' information) [39, 40], it appears that lipid peroxidation was decreased in the NPCs of the Non-R patient and increased in the Mito patient (Figure 2F, Table S3).

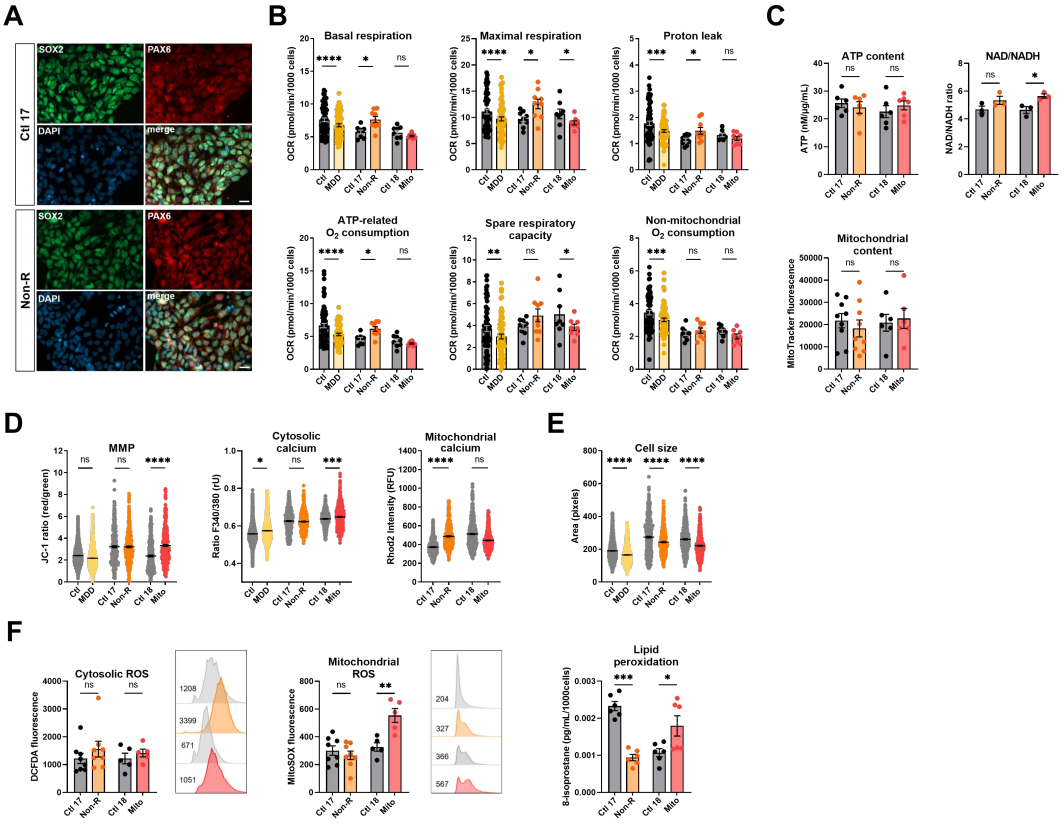

Figure 2. Mitochondrial bioenergetics in neural progenitor cells (NPCs). (A) Typical NPC markers. Representative images show PAX6 and SOX2 are co-expressed by a majority of the NPCs differentiated from Ctl 17 and Non-R patient (see Table S2 for quantification). Scale bar indicates

20 µm. **(B) Mitochondrial respiration.** The oxygen consumption rate (OCR) was measured following the Agilent XF Mito Stress Test protocol. OCR of control and patient NPCs in key respiratory parameters are represented with bar plots of normalized mean OCR values ± SEM. **(C) Bioenergetic parameters.** *ATP content* was measured using a luminescent assay and normalized to protein amount, bar plot shows nM ATP per µg/mL proteins ± SEM. Substrate availability was estimated by measuring the *NAD/NADH ratio* with a colorimetric assay. Bar plots represent mean NAD/NADH ratio ± SEM. *Mitochondrial content* was measured by flow cytometry and is indicated by MitoTracker Green mean fluorescence ± SEM, $1x10^5$ events were recorded for each replicate. **(D) MMP and calcium homeostasis.** *MMP* was measured with the JC-1 dye and is indicated by the fluorescence ratio between JC-1 aggregates (red) over JC-1 monomers (green). Dot plot shows mean red/green ratios ± SEM. *Cytosolic calcium* was measured as the Fura-2 fluorescence ratio F340/380 and is represented as mean ratio ± SEM. *Mitochondrial calcium* levels were measured using Rhod-2/AM and is presented as mean fluorescence intensity, in relative fluorescent unit ± SEM. **(E) Cell size** was analyzed by assessing area (pixels) of Fura-2/AM-loaded cells. Dot plot shows the number of pixels ± SEM. **(F) Oxidative stress indicators.** Cytosolic reactive oxygen species (ROS) and mitochondrial ROS (superoxide) were measured by flow cytometry and are indicated by DCFDA and MitoSOX mean fluorescence, respectively. Bar plots show mean fluorescence ± SEM, $1x10^5$ events were recorded for each replicate. On the right of each graph, with matching colour coding and order, are representative histograms showing fluorescence (x-axis) and cell count (y-axis). Numbers indicate mean fluorescence. *Lipid peroxidation* was estimated by measuring 8-isoprostane concentration in cell culture supernatant and normalized to the number of cells. Bar plots show mean 8-isoprostane concentration in pg/mL/1000 cells ± SEM. Ctl: non-depressed controls cohort; MDD: major depressive disorder cohort; Ctl 17 and Ctl 18: non-depressed controls; Non-R: non-responder patient; Mito: mitochondriopathy patient. All data were analyzed with paired t-test, significant differences were indicated with * ($p<0.05$), ** ($p<0.005$), *** ($p<0.0005$) and **** ($p<0.0001$). Mean, SEM, n and *p*-value are compiled in Table S3.

3.4. Induced astrocytes of patients show altered bioenergetic properties and oxidative stress

To extend our studies on the bioenergetic properties and mitochondrial function in patient cells of the neural lineage, we implemented the differentiation of NPCs to astrocytes according to the protocol of [33]. To verify successful differentiation, we stained against markers typically expressed in mature astrocytes 30 days after starting the differentiation. Immunofluorescent antibody labelling demonstrated expression of GFAP, ALDH1L1, EAAT1, S100β and connexin 43 (Figure 3A, Table S4). Moreover, the presence of ATP-induced wave-like Ca^{2+} signals in the astrocyte culture indicated that the NPCs differentiated to mature astrocytes (Fig S1). In addition to the Mito and Non-R patients and their direct controls, we generated astrocytes from subjects of our MDD and control cohort [29] to use them as a reference in our study (for cohort information, see Table S5).

Basal and maximal respiration, proton leak, the ATP-related and non-mitochondrial oxygen consumption were significantly lower in MDD astrocytes (Figure 3B, Table S4), consistent with findings previously reported in fibroblasts and NPCs. In contrast, the basal and maximal respiration of Non-R astrocytes were reduced compared to its controls. Basal and maximal respiration of the Mito astrocytes were not different from its control (Figure 3B, Table S4). These data indicate that the OXPHOS in astrocytes of Mito and Non-R patient might be affected in a differential and cell-dependent manner.

As in the other cell types, there was no significant difference in the mitochondrial content in astrocyte. However, Mito patient's astrocytes showed significantly decreased ATP concentration (Figure 3C, Table S4).

Representing a further measure of bioenergetic functions, the MMP was decreased in astrocytes from MDD patients and the Mito patient, but significantly increased in the Non-R patient (Figure 3D, Table S4). Regarding Ca^{2+} homeostasis, the MDD cohort astrocytes displayed slightly, yet significantly reduced cytosolic Ca^{2+} levels, whereas there was a marked increase in the Non-R astrocytes, and a significant elevation in the Mito astrocytes (**Fehler! Verweisquelle konnte nicht gefunden werden.**B). Consistent with a decreased MMP, mitochondrial Ca^{2+} levels were lower in the MDD cohort and Mito patient's

cells. In contrast, despite a higher MMP, Non-R astrocytes showed decreased levels of mitochondrial Ca^{2+} as well (Figure 3D, Table S4).

In line with previous observations, cell size was decreased in MDD and Non-R astrocytes. Surprisingly, astrocytes from the Mito patient were found to be larger than those of the corresponding controls (Figure 3E, Table S4).

Cellular ROS showed high variability between groups and were altered in opposite directions in the patients' astrocytes. They were decreased in the Non-R astrocytes but increased in the Mito patient. Mitochondrial superoxide content did not differ (Figure 3F, Table S4).

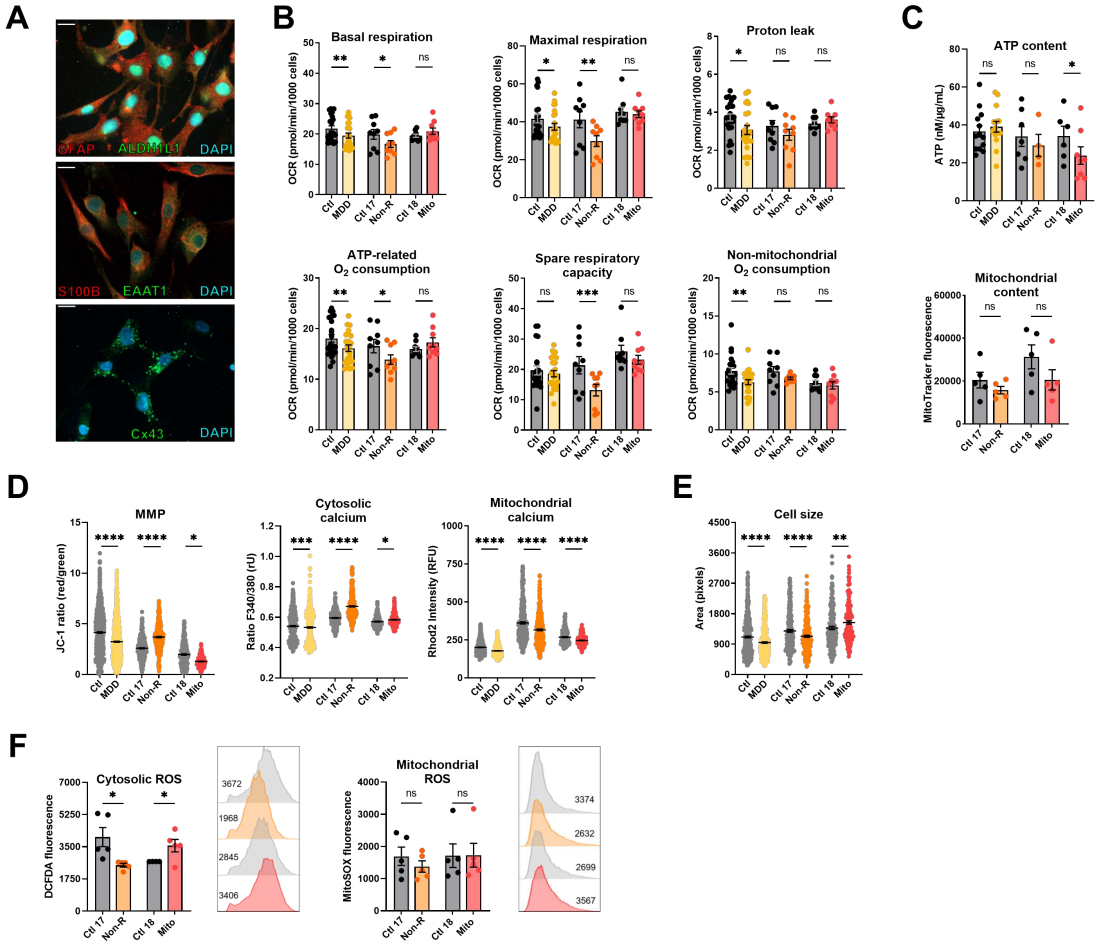

Figure 3. Mitochondrial bioenergetics in astrocytes. (A) Astrocytes markers. Immunofluorescence stainings show that cells express the typical mature astrocytes markers GFAP, ALDH1L1, S100β, EAAT1 and Connexin 43. Scale bar indicates 20 µm. **(B) Mitochondrial respiration.** The oxygen consumption rate (OCR) was measured following the Agilent XF Mito Stress Test protocol. OCR of control and patient astrocytes in key respiratory parameters. Bar plots show normalized mean OCR values ± SEM. **(C) Bioenergetic parameters.** *ATP content* was measured using a luminescent assay and normalized to protein amount, bar plot shows nM ATP per µg/mL proteins ± SEM. *Mitochondrial content* was measured by flow cytometry and is indicated by MitoTracker Green mean fluorescence ± SEM, $1x10^5$ events were recorded for each replicate. **(D) MMP and calcium homeostasis.** *MMP* was measured with the JC-1 dye and is indicated by the fluorescence ratio between JC-1 aggregates (red) over JC-1 monomers (green). Dot plot shows mean red/green ratios ± SEM. *Cytosolic calcium* was measured as the Fura-2 fluorescence ratio F340/380, and is represented as mean ratio ± SEM. *Mitochondrial calcium* levels were measured using Rhod-2/AM and is presented as mean fluorescence intensity, in relative fluorescent unit ± SEM. **(E) Cell size** was analyzed by assessing area (pixels) of Fura-2/AM-loaded cells. Dot plot shows the number of pixels ± SEM. **(F) Oxidative stress indicators.** Cytosolic reactive oxygen species (ROS) and mitochondrial ROS (superoxide) were

measured by flow cytometry and are indicated by DCFDA and MitoSOX mean fluorescence, respectively. Bar plots show mean fluorescence ± SEM, $2x10^4$ events were recorded for each replicate. On the right of each graph, with matching colour coding and order, are representative histograms showing fluorescence (x-axis) and cell count (y-axis). Numbers indicate mean fluorescence. Ctl: non-depressed controls cohort; MDD: major depressive disorder cohort; Ctl 17 and Ctl 18: non-depressed controls; Non-R: non-responder patient; Mito: mitochondriopathy patient. All data were analyzed with paired t-test, significant differences were indicated with * ($p<0.05$), ** ($p<0.005$), *** ($p<0.0005$) and **** ($p<0.0001$). Mean, SEM, n and *p*-value are compiled in Table S4.

3.5. Neurons of patients show altered MMP and Ca^{2+} homeostasis

To investigate functional phenotypes of patient-derived neuronal cells, we differentiated NPCs to cortical-like neurons following the protocol previously used in [29]. We demonstrated successful differentiation by staining against typical neuronal markers and we showed our cultures mostly consist of glutamatergic neurons (Figure 4A, Table S6). To further illustrate the morphology of the neurons, we produced high-resolution electron micrographs, showing a dense neurite network and protrusions (Figure 4B, Table S6). Moreover, our recordings demonstrated that the neurons expressed functional glutamate and $GABA_A$ receptors (FigureS2).

Mitochondrial function in neurons was first investigated by evaluating JC-1 fluorescence as a measure of MMP. Since mitochondria residing in the somas or in the neurites appeared in different focal planes, we separately imaged JC-1 fluorescence by focusing on the relevant structures. The MMP of the Non-R neuronal mitochondria was decreased relative to the control, whereas Mito mitochondria showed increased MMP, especially in the neurites (Figure 4C, Table S6).

Next, we investigated cellular Ca^{2+} homeostasis in the induced neurons. With our experimental setup, evaluation of Ca^{2+} levels was only possible in the soma, but it was carried out in the cytosol and in mitochondria. As the MMP, cytosolic Ca^{2+} levels were decreased in the Non-R neurons. In the Mito neurons, decreased cytosolic Ca^{2+} levels were accompanied by decreased mitochondrial Ca^{2+} levels (Figure 4D, Table S6). Cell size was decreased in the Mito patient's neurons (Figure 4E, Table S6).

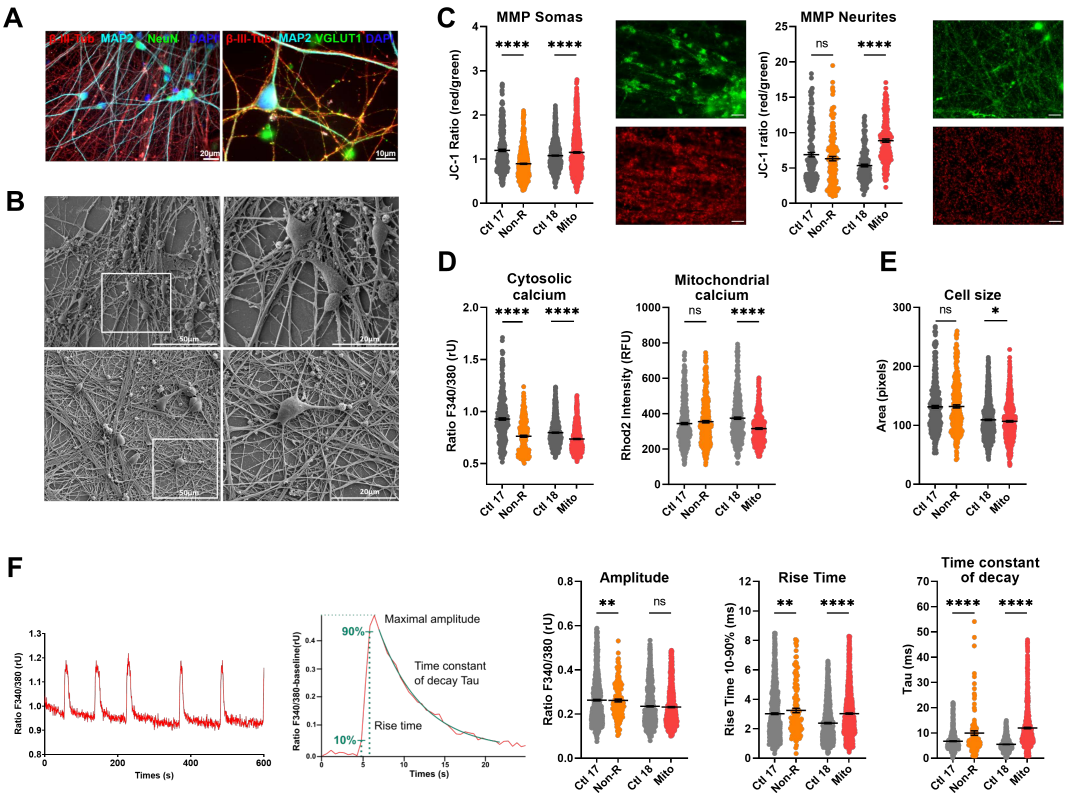

Figure 4. Mitochondrial membrane potential (MMP), calcium homeostasis and dynamics in iPS-Neurons (A) Neuronal markers. Immunofluorescence stainings on neurons revealed that the induced neurons express typical neuronal cytoskeleton protein MAP2 and βIII-Tubulin and neuronal nuclear marker NeuN. VGlut expression suggests that most of the induced neurons are glutamatergic. Scale bars indicate 20 µm or 10µm. **(B) Electron micrographs.** Electron micrographs provide high-resolution visualization of neuronal morphology. Scale bars indicate 50 µm (left) and 20 µm (right) **(C) MMP in somas and neurites.** MMP was measured with the JC-1 dye and is indicated by the fluorescence ratio between JC-1 aggregates (red) over JC-1 monomers (green). Mitochondria from somas and neurites appeared on different focal planes and were therefore imaged separately. Representative images show red and green JC-1 fluorescence in the relevant structure. Scale bar indicates 20 µm. Dot plot shows mean red/green ratios ± SEM. **(D) Calcium homeostasis.** *Cytosolic calcium* was measured as the Fura-2 fluorescence ratio F340/380 and is represented as mean ratio ± SEM. *Mitochondrial calcium* levels were measured using Rhod-2/AM and are presented as mean fluorescence intensity, in relative fluorescent unit ± SEM **(E) Cell size** was analyzed by assessing area (pixels) of Fura-2/AM-loaded cells. Dot plot shows the number of pixels ± SEM **(F) Calcium dynamics.** Spontaneous calcium transients were analyzed in Fura-2/AM-loaded cells. Example traces show representative calcium transients in a neuron (left) and a baseline subtracted calcium peak, illustrating maximal amplitude, rise time between 10 and 90% of maximal amplitude and the exponential fit used to calculate the time constant of decay Tau (right). Graphs show the maximum amplitude of the calcium peaks (ratio 340 nm/380 nm ± SEM), the rise time and the time constant of decay Tau (ms ± SEM). Ctl 17 and Ctl 18: non-depressed controls; Non-R: non-responder patient; Mito: mitochondriopathy patient. All data were analyzed with paired t-test, significant differences were indicated with * ($p<0.05$), ** ($p<0.005$), *** ($p<0.0005$) and **** ($p<0.0001$). Mean, SEM, n and *p*-value are compiled in Table S6.

3.6. Functional properties and the activity of patient-derived neurons are altered

Electrical activity is a hallmark of neuronal function. To investigate biophysical properties of neurons we performed whole-cell patch-clamp recordings of patient-derived and control neurons. We found that the resting membrane potential (RMP) of the Mito neurons was significantly less negative than control, as was the case in neurons from the MDD

cohort. Interestingly, the Non-R neurons showed a significantly more hyperpolarized RMP (Figure 5A, Table S7). It should be noted that the patient neurons had a more negative RMP than the MDD cohort neurons used in [29]. Optimization of the differentiation protocol may have resulted in a more advanced and mature phenotype of the neurons.

Consistent with the results of the MMD cohort, the neurons of the case study patients had a lower electrical capacitance, i.e., they were smaller than those of the corresponding controls (Figure 5A, Table S7).

Analysis of the voltage-gated potassium currents revealed that the current density (pA/pF) was significantly higher in neurons of both the Mito and Non-R patients (Figure 5B, Table S7). The voltage-gated sodium channels of Mito and MDD neurons also showed a significantly higher current density, whereas sodium current densities in Non-R neurons did not differ from its control (Figure 5B, Table S7).

Furthermore, the current-clamp mode was used to adjust the basal membrane potential to approximately -50 mV or -80 mV by current injection, and record the potential fluctuations, which occasionally lead to spontaneous action potentials (APs) (Figure 5C-D, Table S7). Again, the patient neurons showed opposite behavior. The activity of the Mito neurons was significantly increased (higher number of active cells), whereas Non-R neurons were less active (fewer cells showed spontaneous APs, paralleled by a decrease in number of APs in active cells) (Figure 5C-D, Table S7).

The spontaneous APs from Mito neurons were significantly larger and showed smaller full width half maximum (FWHM) time than those of the relevant control (Figure 5F, Table S7). The amplitudes and the FWHM time of Non-R APs were smaller than in the control (Figure5F, Table S7).

Postsynaptic currents (PSCs) recorded in voltage-clamp experiments (at a holding potential of -80 mV) can be considered a measure of synaptic input. Only 30% of Non-R neurons displayed PSCs, while the proportion was 81% in Ctl 17 (**Fehler! Verweisquelle konnte nicht gefunden werden.**A). In contrast, a large proportion of Mito neurons (72%) received synaptic input, although there was no significant difference compared with synaptic activity in Ctl 18 (56%) (Figure 5E, Table S7).

Interestingly, the PSCs of Mito neurons differed in various parameters. They were significantly smaller in amplitude, showed an increased rise time$_{10\text{-}90\%}$ and a prolonged time constant of decay compared to their control (Figure 5G, Table S7). In Non-R neurons, in spite of a small proportion of active cells, PSCs had an increased rise time$_{10\text{-}90\%}$ and larger amplitude (Figure 5G, Table S7).

The electrical activity of the cultured neurons triggered Ca^{2+} signals in the neurons that were analyzed by live-cell imaging using the Ca^{2+}-sensitive dye Fura-2/AM. Interestingly, the rise time$_{10\text{-}90\%}$ and the time constant of decay were increased in the Mito neurons, suggesting prolonged Ca^{2+} signals. However, the risetime was unchanged in the Non-R patient but the time constant of decay was also increased. The amplitudes of the Ca^{2+} transients were not different between the groups (Figure 4F, Table S6).

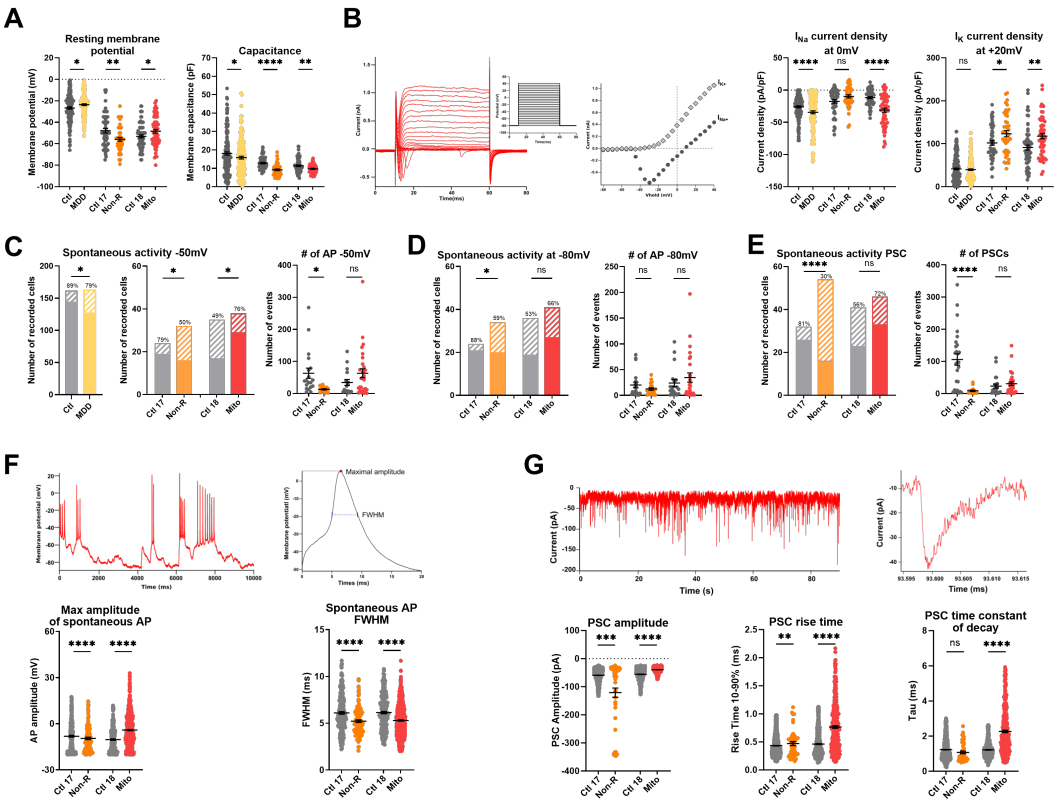

Figure 5. Electrophysiological properties of patients-derived iPS-Neurons. (A) Passive biophysical properties. Resting membrane potential (RMP) and capacitance were recorded immediately after reaching the whole-cell configuration. Dot plot shows mean RMP in mV ± SEM and mean capacitance in pF ± SEM **(B) Sodium and potassium current densities.** Sodium (INa) and potassium (IK) currents were recorded in voltage-clamp mode while holding the membrane potential at -80 mV (Vhold) and depolarizing in steps of 10 mV to provoke the opening of voltage-gated Na^+ and K^+ channels. Example traces show depolarizing steps and the evoked Na^+ and K^+ current, and the resulting IV curve. Currents measurements were normalized to the membrane capacitance to account for cell size variability (current density, pA/pF). Dot plots show mean INa current density at 0 mV in pA/pF ± SEM and mean IK current density at +20 mV in pA/pF ± SEM. **(C and D) Spontaneous action potentials (APs** were recorded in current-clamp while the membrane potential was held at -50 mV **(C)** or -80 mV **(D)**. Spontaneous activity is represented as the proportion of active cells (solid colour), inactive cells (pattern). The percentage of active cells is indicated above each. Dot plots show the mean number of recorded APs ± SEM in case study patients. **(E) Spontaneous post-synaptic currents (PSCs)** were recorded at a holding potential of -80 mV. Left graph shows the proportion of active cells (solid colour), inactive cells (pattern) and the percentage of active cells. Right graph shows the mean number of recorded PSCs ± SEM. **(F) Spontaneous APs analysis**. Spontaneous APs at -80 mV were analyzed individually to extract the maximal amplitude and the full width at half maximum (FWHM). Example traces show spontaneous APs (left) and a single AP trace illustrating amplitude and FWHM (right). Graphs show mean AP amplitude in mV ± SEM and mean FWHM in ms ± SEM. **(G) Post-synaptic currents (PSCs) analysis.** Example traces show spontaneous PSCs (left) and one single PSC (right). Graphs show the maximum amplitude of the PSCs (pA ± SEM), the rise time between 10% and 90% of the maximal amplitude and the time constant of decay Tau (ms ± SEM). Ctl 17 and Ctl 18: non-depressed controls; Non-R: non-responder patient; Mito: mitochondriopathy patient. All data were analyzed with paired t-test, except spontaneous activity, which was analyzed with Fisher's exact test. Significant differences were indicated with * ($p<0.05$), ** ($p<0.005$), *** ($p<0.0005$) and **** ($p<0.0001$). Mean, SEM, n and *p*-value are compiled in Table S7.

A summarized overview of the alterations reported in this study, as well as corresponding results in the MDD cohort from previous studies [28, 29] are provided in Table 2.

Table 2. Overview of results. Main findings are summarized in this table. Arrows represent increases (↗) and decreases (↘), and asterisks reflect the significance of the difference. Equal signs (=) represent an unchanged parameter.

	Non-R			Mito			MDD Cohort		
	Fibro-blasts	NPCs	Astro-cytes	Fibro-blasts	NPCs	Astro-cytes	Fibro-blasts	NPCs	Astro-cytes
Respiration	↗	↗	↘	↘	↘	=	↘	↘	↘
ATP	=	=	=	=	=	↘ *	↘ *	=	=
MMP	=	=	↗ ****	↘ ****	↗ ****	↘ *	↘ ****	=	↘ ****
Cytosolic Ca^{2+}	=	=	↗ ****	=	↗ ***	↗ *	=	↗ *	↘***
Mitochondrial Ca^{2+}	↗ ****	↗ ****	↘ ****	=	= (↘)	↘ ****			↘ ****
Cell size	↘ ****	↘****	↘ ****	↘ *	↘ ****	↗ **	↘ ****	↘****	↘ ****
	Neurons								
MMP somas	↘ ****			↗ ****					
MMP neurites	=			↗ ****					
Cytosolic Ca^{2+}	↘ ****			↘ ****					
Mitochondrial Ca^{2+}	=			↘ ****					
RMP	↗ ** (hyperpolarized)			↘ * (depolarized)			↘ * (depolarized)		
Capacitance	↘ ****			↘ **			↘ *		
$I_{Na+\ 0mV}$ curr. density	=			↘ ****			↘ ****		
$I_{K+\ 20mV}$ curr. density	↗ *			↗ **			=		
Spontaneous activity	-50 mV	-80 mV	PSCs	-50 mV	-80 mV	PSCs	-50 mV		
	↘*	↘*	↘****	↗ *	=	=	↘*		
Spont. AP amplitude	↘ ****			↗ ****					
Spont. AP FWHM	↘ ****			↘ ****					
PSC amplitude	↗ ***			↘ ****					
PSC rise time	↗ **			↗ ****					
PSC decay time (Tau)	=			↗ ****					

4. Discussion

Building on previous work on a cohort of MDD patients [28, 29], the present study constituted a deeper exploration into the ways in which mitochondria can influence cellular function and potentially contribute to the development of depression. This was

achieved by examining closely two atypical patients: a MDD patient who was not responsive to antidepressant treatments (referred to as "Non-R"), and a patient diagnosed with a mitochondriopathy (referred to as "Mito").

As previously reported in the MDD cohort [28, 29], we found significant bioenergetics alterations in both case study patients.

In the Non-R patient, fibroblasts and NPCs showed a significantly increased mitochondrial respiration. Constant mitochondrial content suggested that higher respiration resulted from increased OXPHOS activity. These results appear unexpected, given that MDD, like other psychiatric and neurodegenerative diseases, is known to involve mitochondrial alterations and reduced bioenergetics [9, 10, 41]. However, the high OXPHOS activity observed in these cells was not accompanied by an elevated ATP concentration, and MMP was higher, suggesting an uncoupling of the ETC and the ATP synthase. Notably, an increased proton leak and MMP was observed, which could account for that uncoupling. The adenine nucleotide translocator (ANT) is a major catalyst of basal proton leak in mitochondria [42]. It is conceivable that an altered expression or activity of ANT in the Non-R patient's fibroblasts and NPCs resulted in the higher proton leak observed, which caused a compensatory increase in ETC activity, in a failed attempt to maintain the MMP and ATP production. Importantly, the Non-R patient's increased respiration challenges the mitochondrial hypothesis of MDD, which associates the disorder with decreased respiration. This suggests a revision of the theory to include the possibility of harmful over activation in mitochondrial functions, thus creating a detrimental imbalance. Moreover, consistently with a hyperactive ETC, mitochondrial ROS were significantly increased in the Non-R fibroblasts. Elevated mitochondrial Ca2+ levels in these cells can further increase ROS production and sensitize mitochondria to apoptotic Ca2+-induced mPTP opening [43].

In contrast to fibroblasts and NPCs, mitochondrial respiration in the astrocytes from the Non-R patient was generally reduced. Ca^{2+} is known to stimulate respiration by activating key enzymes in the TCA cycle. In line with this, respiratory activity and mitochondrial Ca^{2+} levels showed a consistent trend in this patient's cells: both increased in fibroblasts and NPCs but decreased in astrocytes. One explanation for the metabolic differences in the Non-R patient's astrocytes could lie in the specificities of astrocytic mitochondrial Ca^{2+} homeostasis. Indeed, astrocytes do not seem to rely on the mitochondrial uniporter (MCU) for Ca^{2+} influx [44], whereas the Na^{+}/Ca^{2+}/lithium exchanger (NCLX) plays a particularly important role in Ca^{2+} efflux [45, 46]. We could hypothesize that the Non-R patient's cells expressed higher amounts of NCLX, resulting in a particularly enhanced Ca^{2+} efflux from astrocytic mitochondria, and, consequently, reduced mitochondrial Ca^{2+} and ETC activity in astrocytes. In contrast, the elevated mitochondrial Ca^{2+} observed in fibroblasts and NPCs from the Non-R patient could result from modulations of MCU expression, a mechanism that would not affect astrocytic mitochondrial Ca^{2+} level.

In the Mito patient, fibroblasts and NPCs showed significantly reduced oxygen consumption rates. This observation is consistent with a reduced function of the electron transport chain (ETC) and OXPHOS in MDD, as we reported previously [28, 29], and as may be assumed for a patient showing signs of a mitochondriopathy. However, no known pathogenic disease-associated variants in nuclear genes were detected by exome sequencing of the Mito patient's fibroblasts, nor by mitochondrial genome sequencing [47]. This could indicate that either a sporadic mutation in one of the mitochondrial genes, or an environmental factor is responsible for the observed phenotype. Additionally, it is impossible to completely exclude any mitochondrial mutation, as mutated mtDNA could be present only in a subset of the total mtDNA population in a tissue (heteroplasmy) [48]. It is also important to note that the analysis of sequence data should not be regarded as a final assessment of the entirety of all genes.

The unchanged mitochondrial content in this patient's cells suggested that lower respiration was due to a decreased OXPHOS activity. However, ATP content remained stable, which suggests a compensatory glycolytic activity that offsets the cost of running energy-intensive processes [49].

In Mito patient's fibroblasts, lipid peroxidation was increased, while glutathione antioxidant system was decreased, suggesting compromised antioxidant defenses. Furthermore, in NPCs from this patient, both mitochondrial superoxide and lipid peroxidation were increased, indicating a high oxidative stress. Low respiration, high superoxide and high MMP together are indicative of reverse electron transfer in these cells [50].

As in the Non-R patient, astrocytes from the Mito patient displayed distinct characteristics. While in the MDD cohort astrocytic respiration was consistently decreased, astrocytes from the Mito patient exhibited unchanged respiration. Moreover, ATP concentration was significantly decreased suggesting alterations in other metabolic pathways. Astrocytes predominantly use glycolysis for energy production [51]. Notably, ROS inhibit various glycolytic enzymes including glyceraldehyde 3-phosphate dehydrogenase (GAPDH), and Hyslop and colleagues demonstrated ROS also directly inhibit ATP synthase without decreasing the respiratory chain capacity [52]. Therefore, we hypothesize that the elevated cytosolic ROS detected by DCFDA in this patient's astrocytes hindered ATP production. Taken together, the absence of an OXPHOS increase despite lower ATP and MMP indicate that astrocytic mitochondria are struggling to meet energy demands efficiently in the Mito patient.

The tight regulation of cytosolic Ca^{2+} levels is critical for cell viability. The endoplasmic reticulum (ER) is the primary Ca^{2+} storage site, and its close interaction with mitochondria at contact sites called mitochondrial associated membranes (MAMs) facilitates significant Ca^{2+} exchanges [53]. Ca^{2+} levels are also maintained by transporters and pumps, such as the Plasma Membrane Ca^{2+} ATPase (PMCA), which use ATP to extrude Ca^{2+} out of the cell. In our study, the main change observed over the different patients and different cell types was a rise in cytosolic Ca^{2+} levels. Interestingly, most instances of increased cytosolic Ca^{2+} were accompanied by decreased respiration. Mankad *et al.* demonstrated that when mitochondrial respiration is altered, even if global ATP concentrations are maintained, PMCA becomes particularly sensitive to small ATP fluctuations [54]. It is therefore plausible that in patients cells exhibiting higher Ca^{2+} levels, perturbations in respiration may have reduced PMCA activity, leading to an intracellular Ca^{2+} rise. Contrastingly, cytosolic Ca^{2+} levels were significantly lower in neurons derived from both patients, which could have implications on neurotransmission, if this decrease is also observed in synaptic terminals. Indeed, lower Ca^{2+} at the synapses can result in lower probability of neurotransmitter release and alter Ca^{2+}-dependent short term plasticity mechanisms [55].

Cytosolic Ca^{2+} dynamics can also impact mitochondrial Ca^{2+} and vice versa. For instance, under stress conditions, mitochondria may release Ca^{2+} into the cytosol as a protective mechanism against apoptosis. A concurrent increased cytosolic Ca^{2+} and decreased mitochondrial Ca^{2+} was observed in astrocytes from both patients. This could reflect cellular stress or result from the unique characteristics of astrocytes concerning mitochondrial Ca^{2+} influx and efflux, as described above. The MMP also impacts mitochondrial Ca^{2+} levels. Here, the mitochondrial Ca^{2+} levels in the analyzed cell lineages do only partially follow the observed MMP or cytosolic Ca^{2+} levels. Nonetheless, it is noteworthy that mitochondrial Ca^{2+} levels were altered in all patients-derived cells, and that the variations consistently mirrored changes in mitochondrial respiration. This aligns with the activating role of Ca^{2+} on OXPHOS [56], and underscores the central role of mitochondria in the cellular anomalies observed in these patient's cells. Similarly, in the Mito patient's neurons, we observed decreased mitochondrial Ca^{2+} despite increased MMP. Considering that ATP concentration is proportional to the rise in mitochondrial Ca^{2+} [57], this observation suggests that the Mito patient's neurons struggle with the dynamic regulation of ATP synthesis. In the Non-R patient's neurons, mitochondrial Ca^{2+} was unchanged but the

MMP was decreased in somatic mitochondria. Due to technical reasons, we were not able to analyze mitochondrial respiration in neurons. However, assuming that decreased MMP reflects decreased OXPHOS rates and subsequent ATP production in somas, insufficient ATP in the soma could affect the neuron's ability to integrate these signals effectively, potentially altering its responsiveness to synaptic inputs [58].

Interestingly, we demonstrated that the size of the patient cells was reduced compared to their healthy controls, when measured as the sum of fluorescent pixels in fibroblasts, NPCs, and astrocytes, and as the electrical capacitance of neurons. This observation is consistent with our earlier findings in NPCs and neurons [29]. The only exception observed were larger astrocytes in the Mito patient, which also differed from other cells by exhibiting elevated cellular ROS. This size increase could therefore result from oxidative stress, as a mechanism to dilute ROS, or as a result of the production of protective proteins to counteract oxidative stress [59]. All other patient astrocytes were consistently smaller than the corresponding controls, so overall, cell size remains a robust symptom/surrogate marker for patient cells. Interestingly, in a recent study where knocking-down the mitochondrial protein TSPO resulted in mitochondrial dysfunctions, a decreased cell size was also consistently observed across different cell types [60]. These findings, in conjunction with ours, suggest a relationship between mitochondrial dysfunction and reduced cell size.

We also demonstrated that biophysical properties and function from Mito and Non-R patients neurons differ from their corresponding controls. A striking feature of both patient-derived neurons was the markedly increased density of K^+ currents, which allows for efficient post-AP repolarization of the membrane potential.

In Non-R patient's neurons, a hyperpolarized RMP with constant Na^+ current density suggests a bigger hurdle to reach the AP threshold. Consistently, spontaneous activity was significantly lower, both at -50 and -80 mV, there was a lower frequency of AP in active cells, and the APs observed were smaller and narrower. Moreover, postsynaptic currents (PSCs) were drastically altered, with a much smaller fraction of active cells, a drop in event frequency, and the PSCs had extended rise time. Altered synaptic transmission can result in altered synaptic plasticity, a hallmark of MDD [61]. Interestingly, Vadodaria *et al.* reported altered neurite growth and morphology in neurons derived from serotonin reuptake inhibitors (SSRI) non-responder depressed patients. These changes were associated with lowered expression of key Protocadherin alpha genes [62]. Such alterations in the Non-R patient could influence network activity and explain the observed decreases in spontaneous APs and PSCs. Overall, our observations in the Non-R patient's neurons point to a significant shift in excitability and neuronal transmission. These changes suggest that cortical neurons in the Non-R patient might be less responsive to serotonergic signals due to their hyperpolarization. This could mean that these neurons are less receptive to the increased serotonergic signaling resulting from antidepressant treatment, potentially explaining the Non-R patient's lack of response to such treatments.

Mito patient's neurons exhibited many similar characteristics to neurons from the MDD cohort patients. Both displayed depolarized RMP, which together with lower capacitance could suggest a compromised energy supply due to mitochondrial dysfunction. This is underscored by the substantial energy demands of maintaining RMP and the pivotal role of mitochondrial biogenesis in axonal growth [63]. Furthermore, the depolarized RMP in Mito and MDD neurons was closer to the AP threshold, and increased Na+ currents further promoted depolarization. In the Mito patient, this led to a high proportion of neurons showing spontaneous APs at -50 mV. The APs were taller, yet narrower, consistent with changes in Na+ and K+ currents. Hyperexcitability is a common feature of mitochondrial disorders, especially in MELAS [64] and MERRF [65]. Supporting this, mice models with induced mitochondrial dysfunction by conditional knock-out of critical mitochondrial proteins showed increased excitability in both glutamatergic neurons [66] and

serotonergic neurons [67]. While these studies did not identify the exact cause of hyperexcitability, both suggested a potential disruption in Ca2+ homeostasis, with defective Ca2+ accumulation in mitochondria following depolarization. This aligns with the decreased mitochondrial Ca2+ levels observed in the Mito patient's neurons.

Additionally, spontaneous PSCs had significantly lower amplitude and longer rise and decay time, potentially indicating changes in neurotransmitter release. There is increasing evidence linking mitochondrial dysfunction to synaptic transmission failures in Alzheimer's disease. Notably, patients with early-stage Alzheimer's disease show synaptic mitochondria issues even before significant synaptic damage occurs [68]. Considering this, it is plausible that the synaptic transmission alterations observed in the Mito patient stem from impairments of neuronal mitochondria.

5. Limitations

Interindividual differences could be exacerbated by the differences in the age of the patient/control pairs. Supporting this assumption, we observed a positive correlation of various functional parameters, such as maximal oxygen consumption and spare respiratory capacity, with age in the non-depressed control cohort (n=16, Figure S3). Furthermore, it has been widely demonstrated that there is an age-associated increase in steady-state concentrations of lipid peroxidation products [40] and oxidative DNA damage (OH8dG; [39]).

In view of the interindividual variability in direct comparison of two subjects, we aimed to relate the data of the presented case study also to the data obtained from a larger cohort of MDD patients and controls, whenever possible. However, we recognize that our results reflect the observations of independent individuals and cannot be interpreted as generally applicable interpretations of MD and TRD.

The MDD patients from our cohort study were considered no longer depressed at the time of the biopsies, as assessed with the Hamilton-rating scale for Depression. Indeed, the patients' scores were 10.8 ± 1.9, which is recognized as subthreshold, mild depression [69]. Therefore, our study does not address depressive state, but rather trait markers.

No clear diagnosis on the Mito patient was available, although several clinical parameters, as well as our initial respiratory measurements indicated a mitochondria-associated disease.

Limitations exist in sequencing data analysis, for example in the detection of low-grade mosaics, of repeat expansions, of balanced changes (translocations and inversions), and in the calling accuracy of larger Indels. Furthermore, in exome sequencing, variants in non-enriched regions (untranslated regions, introns, promoter, and enhancer regions) cannot be detected. In general, accuracy is limited for all variant types in regions with high sequence homology or low complexity or with other technical challenges.

Reprogramming of fibroblasts may affect the expression of disease-associated epigenetic memories. However, we have already shown that functional mitochondrial phenotypes are transmitted (at least partially) to the iPS-derived lineages [29, 70].

6. Conclusions

In the non-responder patient (Non-R), fibroblasts and NPCs exhibited markedly increased respiration but constant MMP, suggesting proton leak, potentially via the adenine nucleoside transporter. The high OXPHOS activity could result from the starkly elevated mitochondrial Ca^{2+} and led to high mitochondrial ROS. In neurons from this patient, evidence suggested compromised synaptic transmission. MMP was decreased in the soma, basal calcium was lowered, calcium peaks were extended, and spontaneous postsynaptic currents were markedly reduced. The Non-R patient's neurons also displayed decreased

excitability, attributed to the hyperpolarization of the resting membrane potential (RMP), leading to fewer spontaneous action potentials. This altered network activity might be linked to altered neurite growth. Overall, these changes might make the patient's cortical neurons less responsive to serotonergic neurons innervating the cortex. This could potentially explain the patient's non-responsiveness to serotonin-increasing antidepressant treatments.

Interestingly, cells from this Non-R patient often presented a contrasting functional phenotype, which starkly deviated from the expected, thus highlighting deeper layers of complexity in the disease and pointing to the involvement of different mechanisms in the etiology of depression. The bioenergetics hypothesis of MDD seems to be more nuanced than a strict decrease of function, and to also encompass an over activation of certain mitochondrial functions, thereby creating a detrimental imbalance.

In the mitochondriopathy patient (Mito), generally impaired bioenergetics functions were evident, characterized by a decreased respiration and depolarized MMP, whereas oxidative stress indicators were high. In NPCs, the combination of high MMP, low respiration and elevated ROS suggested reverse electron transport, potentially impacting cell function and neuronal differentiation. Neurons from the Mito patient had high MMP and exhibited hyperexcitability, linked to a depolarized RMP and increased sodium current density. The decreased mitochondrial calcium implied that Mito neurons struggled adjusting to the energy demands of neurotransmission and coincided with reduced cytosolic calcium and prolonged calcium peak durations, leading to diminished and slower synaptic currents.

It is important to highlight that cells derived from this Mito patient mirrored the (dys)function observed in the MDD cohort cells in many cellular and mitochondrial functional parameters, supporting the hypothesis that mitochondria play a crucial role in the pathophysiology of depression. Moreover, valuable insights into prospective research directions emerge from these findings, particularly focusing on the oxidative stress/antioxidant dynamics and the kinetics of spontaneous neuronal activity in a MDD patient cohort.

Finally, cells from both patients were overall smaller in size. Given mitochondria's role in determining optimal cell size, this could be a marker for mitochondrial dysfunction.

Overall, the present study emphasizes the importance of closely investigating atypical patients to gain a more comprehensive understanding of the multifaceted pathophysiology of MDD.

Supplementary Materials: The following supporting information can be downloaded at: www.mdpi.com/xxx/s1, Figure S1**:** Calcium transients in astrocytes; Figure S2: Glutamate and GABA response in current-clamp; Figure S3. Electrophysiological recordings in iPS-neurons; Figure S4. Correlation between age and mitochondrial respiration; Table S1. Mitochondrial bioenergetics in fibroblasts; Table S2. Neural progenitor cells markers PAX6 and SOX2; Table S3. Mitochondrial bioenergetics in neural progenitor cells (NPCs); Table S4. Mitochondrial bioenergetics in astrocytes; Table S5. Patients and controls information – Astrocytes cohort; Table S6. Mitochondrial membrane potential (MMP), calcium homeostasis and dynamics in neurons; Table S7. Electrophysiological properties of patients-derived neurons.

Author Contributions: Conceptualization, Iseline Cardon and Christian Wetzel; Formal analysis, Iseline Cardon, Sonja Grobecker, Selin Kuecuekoktay, Stefanie Bader, Bernhard Weber, Heidi Stoehr, Marcus Hoering, Gerhard Liebisch, Frank Braun, Tanja Rothammer-Hampl, Markus Riemenschneider, Vladimir Milenkovic and Christian Wetzel; Funding acquisition, Christian Wetzel; Investigation, Iseline Cardon, Sonja Grobecker, Selin Kuecuekoktay, Stefanie Bader, Tatjana Jahner, Marcus Hoering, Gerhard Liebisch, Frank Braun, Tanja Rothammer-Hampl, Vladimir Milenkovic and Christian Wetzel; Methodology, Stefanie Bader, Caroline Nothdurfter, Kevin Koschitzki, Mark Berneburg, Bernhard Weber, Heidi Stoehr, Marcus Hoering, Gerhard Liebisch, Frank Braun, Tanja

Rothammer-Hampl, Markus Riemenschneider and Vladimir Milenkovic; Project administration, Christian Wetzel; Resources, Caroline Nothdurfter, Kevin Koschitzki and Mark Berneburg; Supervision, Christian Wetzel; Writing – original draft, Iseline Cardon and Christian Wetzel; Writing – review & editing, Rainer Rupprecht.

Funding: The work has been supported by the Deutsche Forschungsgemeinschaft (DFG, German Research Foundation) project number GRK2174 to CHW and IC, and the Bavarian State Ministry of Science and the Arts (Bavarian Research Networks ForIPS and ForInter, grants to MJR).

Institutional Review Board Statement: Not applicable

Informed Consent Statement: Informed consent was obtained from all subjects involved in the study.

Data Availability Statement: Data is contained within the article and supplementary material.

Acknowledgments: The authors would like to thank Richard Warth for providing access to the Seahorse device.

Conflicts of Interest: The authors declare no conflict of interest.

References

1. Ferrari, A. J.; Charlson, F. J.; Norman, R. E.; Patten, S. B.; Freedman, G.; Murray, C. J.; Vos, T.; Whiteford, H. A., Burden of depressive disorders by country, sex, age, and year: findings from the global burden of disease study 2010. *PLoS Med* **2013,** 10, (11), e1001547.
2. Liu, Q.; He, H.; Yang, J.; Feng, X.; Zhao, F.; Lyu, J., Changes in the global burden of depression from 1990 to 2017: Findings from the Global Burden of Disease study. *J Psychiatr Res* **2020,** 126, 134-140.
3. Organization, W. H., World mental health report: transforming mental health for all. In World Health Organization: 2022.
4. Liu, W.; Ge, T.; Leng, Y.; Pan, Z.; Fan, J.; Yang, W.; Cui, R., The Role of Neural Plasticity in Depression: From Hippocampus to Prefrontal Cortex. *Neural Plast* **2017,** 2017, 6871089.
5. Casarotto, P. C.; Girych, M.; Fred, S. M.; Kovaleva, V.; Moliner, R.; Enkavi, G.; Biojone, C.; Cannarozzo, C.; Sahu, M. P.; Kaurinkoski, K.; Brunello, C. A.; Steinzeig, A.; Winkel, F.; Patil, S.; Vestring, S.; Serchov, T.; Diniz, C.; Laukkanen, L.; Cardon, I.; Antila, H.; Rog, T.; Piepponen, T. P.; Bramham, C. R.; Normann, C.; Lauri, S. E.; Saarma, M.; Vattulainen, I.; Castren, E., Antidepressant drugs act by directly binding to TRKB neurotrophin receptors. *Cell* **2021,** 184, (5), 1299-1313 e19.
6. Fava, M.; Rush, A. J., Current status of augmentation and combination treatments for major depressive disorder: a literature review and a proposal for a novel approach to improve practice. *Psychother Psychosom* **2006,** 75, (3), 139-53.
7. El-Hage, W.; Leman, S.; Camus, V.; Belzung, C., Mechanisms of antidepressant resistance. *Front Pharmacol* **2013,** 4, 146.
8. Moretti, A.; Gorini, A.; Villa, R. F., Affective disorders, antidepressant drugs and brain metabolism. *Mol Psychiatry* **2003,** 8, (9), 773-85.
9. Klinedinst, N. J.; Regenold, W. T., A mitochondrial bioenergetic basis of depression. *J Bioenerg Biomembr* **2015,** 47, (1-2), 155-71.
10. Manji, H.; Kato, T.; Di Prospero, N. A.; Ness, S.; Beal, M. F.; Krams, M.; Chen, G., Impaired mitochondrial function in psychiatric disorders. *Nat Rev Neurosci* **2012,** 13, (5), 293-307.
11. Gardner, A.; Boles, R. G., Beyond the serotonin hypothesis: mitochondria, inflammation and neurodegeneration in major depression and affective spectrum disorders. *Prog Neuropsychopharmacol Biol Psychiatry* **2011,** 35, (3), 730-43.
12. Monzel, A. S.; Enriquez, J. A.; Picard, M., Multifaceted mitochondria: moving mitochondrial science beyond function and dysfunction. *Nat Metab* **2023,** 5, (4), 546-562.
13. Berndt, N.; Holzhutter, H. G., The high energy demand of neuronal cells caused by passive leak currents is not a waste of energy. *Cell Biochem Biophys* **2013,** 67, (2), 527-35.

14. Gorman, G. S.; Chinnery, P. F.; DiMauro, S.; Hirano, M.; Koga, Y.; McFarland, R.; Suomalainen, A.; Thorburn, D. R.; Zeviani, M.; Turnbull, D. M., Mitochondrial diseases. *Nat Rev Dis Primers* **2016,** 2, 16080.
15. Schaefer, A. M.; McFarland, R.; Blakely, E. L.; He, L.; Whittaker, R. G.; Taylor, R. W.; Chinnery, P. F.; Turnbull, D. M., Prevalence of mitochondrial DNA disease in adults. *Ann Neurol* **2008,** 63, (1), 35-9.
16. Koenig, M. K., Presentation and diagnosis of mitochondrial disorders in children. *Pediatr Neurol* **2008,** 38, (5), 305-13.
17. Finsterer, J., Central nervous system manifestations of mitochondrial disorders. *Acta Neurol Scand* **2006,** 114, (4), 217-38.
18. Morava, E.; Gardeitchik, T.; Kozicz, T.; de Boer, L.; Koene, S.; de Vries, M. C.; McFarland, R.; Roobol, T.; Rodenburg, R. J.; Verhaak, C. M., Depressive behaviour in children diagnosed with a mitochondrial disorder. *Mitochondrion* **2010,** 10, (5), 528-33.
19. Fattal, O.; Link, J.; Quinn, K.; Cohen, B. H.; Franco, K., Psychiatric comorbidity in 36 adults with mitochondrial cytopathies. *CNS Spectr* **2007,** 12, (6), 429-38.
20. Anglin, R. E.; Tarnopolsky, M. A.; Mazurek, M. F.; Rosebush, P. I., The psychiatric presentation of mitochondrial disorders in adults. *J Neuropsychiatry Clin Neurosci* **2012,** 24, (4), 394-409.
21. Riquin, E.; Duverger, P.; Cariou, C.; Barth, M.; Prouteau, C.; Van Bogaert, P.; Bonneau, D.; Roy, A., Neuropsychological and Psychiatric Features of Children and Adolescents Affected With Mitochondrial Diseases: A Systematic Review. *Front Psychiatry* **2020,** 11, 747.
22. Chan, S. T.; McCarthy, M. J.; Vawter, M. P., Psychiatric drugs impact mitochondrial function in brain and other tissues. *Schizophr Res* **2020,** 217, 136-147.
23. Gardner, A.; Johansson, A.; Wibom, R.; Nennesmo, I.; von Dobeln, U.; Hagenfeldt, L.; Hallstrom, T., Alterations of mitochondrial function and correlations with personality traits in selected major depressive disorder patients. *J Affect Disord* **2003,** 76, (1-3), 55-68.
24. Hroudova, J.; Fisar, Z., Control mechanisms in mitochondrial oxidative phosphorylation. *Neural Regen Res* **2013,** 8, (4), 363-75.
25. Sjovall, F.; Ehinger, J. K.; Marelsson, S. E.; Morota, S.; Frostner, E. A.; Uchino, H.; Lundgren, J.; Arnbjornsson, E.; Hansson, M. J.; Fellman, V.; Elmer, E., Mitochondrial respiration in human viable platelets--methodology and influence of gender, age and storage. *Mitochondrion* **2013,** 13, (1), 7-14.
26. Karabatsiakis, A.; Bock, C.; Salinas-Manrique, J.; Kolassa, S.; Calzia, E.; Dietrich, D. E.; Kolassa, I. T., Mitochondrial respiration in peripheral blood mononuclear cells correlates with depressive subsymptoms and severity of major depression. *Transl Psychiatry* **2014,** 4, (6), e397.
27. Garbett, K. A.; Vereczkei, A.; Kalman, S.; Wang, L.; Korade, Z.; Shelton, R. C.; Mirnics, K., Fibroblasts from patients with major depressive disorder show distinct transcriptional response to metabolic stressors. *Transl Psychiatry* **2015,** 5, (3), e523.
28. Kuffner, K.; Triebelhorn, J.; Meindl, K.; Benner, C.; Manook, A.; Sudria-Lopez, D.; Siebert, R.; Nothdurfter, C.; Baghai, T. C.; Drexler, K.; Berneburg, M.; Rupprecht, R.; Milenkovic, V. M.; Wetzel, C. H., Major Depressive Disorder is Associated with Impaired Mitochondrial Function in Skin Fibroblasts. *Cells* **2020,** 9, (4), 884.
29. Triebelhorn, J.; Cardon, I.; Kuffner, K.; Bader, S.; Jahner, T.; Meindl, K.; Rothhammer-Hampl, T.; Riemenschneider, M. J.; Drexler, K.; Berneburg, M.; Nothdurfter, C.; Manook, A.; Brochhausen, C.; Baghai, T. C.; Hilbert, S.; Rupprecht, R.; Milenkovic, V. M.; Wetzel, C. H., Induced neural progenitor cells and iPS-neurons from major depressive disorder patients show altered bioenergetics and electrophysiological properties. *Mol Psychiatry* **2022**.
30. Rajkowska, G.; Stockmeier, C. A., Astrocyte pathology in major depressive disorder: insights from human postmortem brain tissue. *Curr Drug Targets* **2013,** 14, (11), 1225-36.
31. Berlim, M. T.; Turecki, G., What is the meaning of treatment resistant/refractory major depression (TRD)? A systematic review of current randomized trials. *Eur Neuropsychopharmacol* **2007,** 17, (11), 696-707.

32. Yan, Y.; Shin, S.; Jha, B. S.; Liu, Q.; Sheng, J.; Li, F.; Zhan, M.; Davis, J.; Bharti, K.; Zeng, X.; Rao, M.; Malik, N.; Vemuri, M. C., Efficient and rapid derivation of primitive neural stem cells and generation of brain subtype neurons from human pluripotent stem cells. *Stem Cells Transl Med* **2013,** 2, (11), 862-70.
33. Tcw, J.; Wang, M.; Pimenova, A. A.; Bowles, K. R.; Hartley, B. J.; Lacin, E.; Machlovi, S. I.; Abdelaal, R.; Karch, C. M.; Phatnani, H.; Slesinger, P. A.; Zhang, B.; Goate, A. M.; Brennand, K. J., An Efficient Platform for Astrocyte Differentiation from Human Induced Pluripotent Stem Cells. *Stem Cell Reports* **2017,** 9, (2), 600-614.
34. Milenkovic, V. M.; Slim, D.; Bader, S.; Koch, V.; Heinl, E. S.; Alvarez-Carbonell, D.; Nothdurfter, C.; Rupprecht, R.; Wetzel, C. H., CRISPR-Cas9 Mediated TSPO Gene Knockout alters Respiration and Cellular Metabolism in Human Primary Microglia Cells. *Int J Mol Sci* **2019,** 20, (13), 3359.
35. Schindelin, J.; Arganda-Carreras, I.; Frise, E.; Kaynig, V.; Longair, M.; Pietzsch, T.; Preibisch, S.; Rueden, C.; Saalfeld, S.; Schmid, B.; Tinevez, J. Y.; White, D. J.; Hartenstein, V.; Eliceiri, K.; Tomancak, P.; Cardona, A., Fiji: an open-source platform for biological-image analysis. *Nat Methods* **2012,** 9, (7), 676-82.
36. Takahashi, K.; Tanabe, K.; Ohnuki, M.; Narita, M.; Ichisaka, T.; Tomoda, K.; Yamanaka, S., Induction of pluripotent stem cells from adult human fibroblasts by defined factors. *Cell* **2007,** 131, (5), 861-72.
37. Okita, K.; Matsumura, Y.; Sato, Y.; Okada, A.; Morizane, A.; Okamoto, S.; Hong, H.; Nakagawa, M.; Tanabe, K.; Tezuka, K.; Shibata, T.; Kunisada, T.; Takahashi, M.; Takahashi, J.; Saji, H.; Yamanaka, S., A more efficient method to generate integration-free human iPS cells. *Nat Methods* **2011,** 8, (5), 409-12.
38. Zhang, X.; Huang, C. T.; Chen, J.; Pankratz, M. T.; Xi, J.; Li, J.; Yang, Y.; Lavaute, T. M.; Li, X. J.; Ayala, M.; Bondarenko, G. I.; Du, Z. W.; Jin, Y.; Golos, T. G.; Zhang, S. C., Pax6 is a human neuroectoderm cell fate determinant. *Cell Stem Cell* **2010,** 7, (1), 90-100.
39. Mecocci, P.; Fano, G.; Fulle, S.; MacGarvey, U.; Shinobu, L.; Polidori, M. C.; Cherubini, A.; Vecchiet, J.; Senin, U.; Beal, M. F., Age-dependent increases in oxidative damage to DNA, lipids, and proteins in human skeletal muscle. *Free Radic Biol Med* **1999,** 26, (3-4), 303-8.
40. Pratico, D., Lipid peroxidation and the aging process. *Sci Aging Knowledge Environ* **2002,** 2002, (50), re5.
41. Rossi, A.; Pizzo, P., Mitochondrial bioenergetics and neurodegeneration: a paso doble. *Neural Regen Res* **2021,** 16, (4), 686-687.
42. Brand, M. D.; Pakay, J. L.; Ocloo, A.; Kokoszka, J.; Wallace, D. C.; Brookes, P. S.; Cornwall, E. J., The basal proton conductance of mitochondria depends on adenine nucleotide translocase content. *Biochem J* **2005,** 392, (Pt 2), 353-62.
43. Drahota, Z.; Endlicher, R.; Stankova, P.; Rychtrmoc, D.; Milerova, M.; Cervinkova, Z., Characterization of calcium, phosphate and peroxide interactions in activation of mitochondrial swelling using derivative of the swelling curves. *J Bioenerg Biomembr* **2012,** 44, (3), 309-15.
44. Huntington, T. E.; Srinivasan, R., Astrocytic mitochondria in adult mouse brain slices show spontaneous calcium influx events with unique properties. *Cell Calcium* **2021,** 96, 102383.
45. Parnis, J.; Montana, V.; Delgado-Martinez, I.; Matyash, V.; Parpura, V.; Kettenmann, H.; Sekler, I.; Nolte, C., Mitochondrial exchanger NCLX plays a major role in the intracellular Ca2+ signaling, gliotransmission, and proliferation of astrocytes. *J Neurosci* **2013,** 33, (17), 7206-19.
46. Palty, R.; Silverman, W. F.; Hershfinkel, M.; Caporale, T.; Sensi, S. L.; Parnis, J.; Nolte, C.; Fishman, D.; Shoshan-Barmatz, V.; Herrmann, S.; Khananshvili, D.; Sekler, I., NCLX is an essential component of mitochondrial Na+/Ca2+ exchange. *Proc Natl Acad Sci U S A* **2010,** 107, (1), 436-41.
47. Fernandez-Vizarra, E.; Zeviani, M., Mitochondrial disorders of the OXPHOS system. *FEBS Lett* **2021,** 595, (8), 1062-1106.
48. Rai, P. K.; Craven, L.; Hoogewijs, K.; Russell, O. M.; Lightowlers, R. N., Advances in methods for reducing mitochondrial DNA disease by replacing or manipulating the mitochondrial genome. *Essays Biochem* **2018,** 62, (3), 455-465.

49. Liemburg-Apers, D. C.; Schirris, T. J.; Russel, F. G.; Willems, P. H.; Koopman, W. J., Mitoenergetic Dysfunction Triggers a Rapid Compensatory Increase in Steady-State Glucose Flux. *Biophys J* **2015,** 109, (7), 1372-86.
50. Murphy, M. P., How mitochondria produce reactive oxygen species. *Biochemical Journal* **2009,** 417, 1-13.
51. Rose, J.; Brian, C.; Pappa, A.; Panayiotidis, M. I.; Franco, R., Mitochondrial Metabolism in Astrocytes Regulates Brain Bioenergetics, Neurotransmission and Redox Balance. *Front Neurosci* **2020,** 14, 536682.
52. Hyslop, P. A.; Hinshaw, D. B.; Halsey, W. A.; Schraufstätter, I. U.; Sauerheber, R. D.; Spragg, R. G.; Jackson, J. H.; Cochrane, C. G., Mechanisms of oxidant-mediated cell injury. The glycolytic and mitochondrial pathways of ADP phosphorylation are major intracellular targets inactivated by hydrogen peroxide. *Journal of Biological Chemistry* **1988,** 263, (4), 1665-1675.
53. Pizzo, P.; Pozzan, T., Mitochondria–endoplasmic reticulum choreography: structure and signaling dynamics. *Trends in Cell Biology* **2007,** 17, (10), 511-517.
54. Mankad, P.; James, A.; Siriwardena, A. K.; Elliott, A. C.; Bruce, J. I. E., Insulin Protects Pancreatic Acinar Cells from Cytosolic Calcium Overload and Inhibition of Plasma Membrane Calcium Pump*. *Journal of Biological Chemistry* **2012,** 287, (3), 1823-1836.
55. Neher, E.; Sakaba, T., Multiple roles of calcium ions in the regulation of neurotransmitter release. *Neuron* **2008,** 59, (6), 861-72.
56. Gellerich, F. N.; Gizatullina, Z.; Trumbeckaite, S.; Nguyen, H. P.; Pallas, T.; Arandarcikaite, O.; Vielhaber, S.; Seppet, E.; Striggow, F., The regulation of OXPHOS by extramitochondrial calcium. *Biochim Biophys Acta* **2010,** 1797, (6-7), 1018-27.
57. Jouaville, L. S.; Pinton, P.; Bastianutto, C.; Rutter, G. A.; Rizzuto, R., Regulation of mitochondrial ATP synthesis by calcium: evidence for a long-term metabolic priming. *Proc Natl Acad Sci U S A* **1999,** 96, (24), 13807-12.
58. Magee, J. C., Dendritic integration of excitatory synaptic input. *Nat Rev Neurosci* **2000,** 1, (3), 181-90.
59. Reeg, S.; Jung, T.; Castro, J. P.; Davies, K. J. A.; Henze, A.; Grune, T., The molecular chaperone Hsp70 promotes the proteolytic removal of oxidatively damaged proteins by the proteasome. *Free Radical Biology and Medicine* **2016,** 99, 153-166.
60. Bader, S.; Wurfel, T.; Jahner, T.; Nothdurfter, C.; Rupprecht, R.; Milenkovic, V. M.; Wetzel, C. H., Impact of Translocator Protein 18 kDa (TSPO) Deficiency on Mitochondrial Function and the Inflammatory State of Human C20 Microglia Cells. *Cells* **2023,** 12, (6).
61. Vose, L. R.; Stanton, P. K., Synaptic Plasticity, Metaplasticity and Depression. *Curr Neuropharmacol* **2017,** 15, (1), 71-86.
62. Vadodaria, K. C.; Ji, Y.; Skime, M.; Paquola, A.; Nelson, T.; Hall-Flavin, D.; Fredlender, C.; Heard, K. J.; Deng, Y.; Le, A. T.; Dave, S.; Fung, L.; Li, X.; Marchetto, M. C.; Weinshilboum, R.; Gage, F. H., Serotonin-induced hyperactivity in SSRI-resistant major depressive disorder patient-derived neurons. *Mol Psychiatry* **2019,** 24, (6), 795-807.
63. Vaarmann, A.; Mandel, M.; Zeb, A.; Wareski, P.; Liiv, J.; Kuum, M.; Antsov, E.; Liiv, M.; Cagalinec, M.; Choubey, V.; Kaasik, A., Mitochondrial biogenesis is required for axonal growth. *Development* **2016,** 143, (11), 1981-92.
64. Sproule, D. M.; Kaufmann, P., Mitochondrial encephalopathy, lactic acidosis, and strokelike episodes: basic concepts, clinical phenotype, and therapeutic management of MELAS syndrome. *Ann N Y Acad Sci* **2008,** 1142, 133-58.
65. Lorenzoni, P. J.; Scola, R. H.; Kay, C. S.; Silvado, C. E.; Werneck, L. C., When should MERRF (myoclonus epilepsy associated with ragged-red fibers) be the diagnosis? *Arq Neuropsiquiatr* **2014,** 72, (10), 803-11.
66. De La Rossa, A.; Laporte, M. H.; Astori, S.; Marissal, T.; Montessuit, S.; Sheshadri, P.; Ramos-Fernández, E.; Mendez, P.; Khani, A.; Quairiaux, C.; Taylor, E. B.; Rutter, J.; Nunes, J. M.; Carleton, A.; Duchen, M. R.; Sandi, C.; Martinou, J.-C., Paradoxical neuronal hyperexcitability in a mouse model of mitochondrial pyruvate import deficiency. *eLife* **2022,** 11, e72595.
67. Kato, T. M.; Kubota-Sakashita, M.; Fujimori-Tonou, N.; Saitow, F.; Fuke, S.; Masuda, A.; Itohara, S.; Suzuki, H.; Kato, T., Ant1 mutant mice bridge the mitochondrial and serotonergic dysfunctions in bipolar disorder. *Mol Psychiatry* **2018,** 23, (10), 2039-2049.

68. Guo, L.; Tian, J.; Du, H., Mitochondrial Dysfunction and Synaptic Transmission Failure in Alzheimer's Disease. *J Alzheimers Dis* **2017,** 57, (4), 1071-1086.

69. Zimmerman, M.; Martinez, J. H.; Young, D.; Chelminski, I.; Dalrymple, K., Severity classification on the Hamilton depression rating scale. *Journal of Affective Disorders* **2013,** 150, (2), 384-388.

70. Kim, K.; Doi, A.; Wen, B.; Ng, K.; Zhao, R.; Cahan, P.; Kim, J.; Aryee, M. J.; Ji, H.; Ehrlich, L. I.; Yabuuchi, A.; Takeuchi, A.; Cunniff, K. C.; Hongguang, H.; McKinney-Freeman, S.; Naveiras, O.; Yoon, T. J.; Irizarry, R. A.; Jung, N.; Seita, J.; Hanna, J.; Murakami, P.; Jaenisch, R.; Weissleder, R.; Orkin, S. H.; Weissman, I. L.; Feinberg, A. P.; Daley, G. Q., Epigenetic memory in induced pluripotent stem cells. *Nature* **2010,** 467, (7313), 285-90.

Supplementary Files

This is a list of supplementary files associated with this preprint. Click to download.

- Supplement.pdf